Modelling & Dynamic Analysis of Wind Turbine Blades

by

Mr. Viswa Teja Vanapalli

(Roll No: 213ME1397)

Under the guidance of

Dr. (Prof.) J. Srinivas

Department of Mechanical Engineering,
National Institute of Technology, Rourkela,
Rourkela – 769008, Odisha, India.

Modelling & Dynamic Analysis of Wind Turbine Blades

A thesis submitted in partial fulfilment of the

requirements for the degree of

Master of Technology

in

Machine Design and Analysis

by

Mr. Viswa Teja Vanapalli

(Roll No: 213ME1397)

Under the guidance of

Dr. (Prof.) J. Srinivas

Department of Mechanical Engineering,
National Institute of Technology, Rourkela,
Rourkela – 769008, Odisha, India.

NATIONAL INSTITUTE OF TECHNOLOGY, ROURKELA

CERTIFICATE

This is to certify that the thesis entitled, "***Modelling &Dynamic Analysis of Wind Turbine Blades***" submitted by ***Mr. Viswa Teja Vanapalli (213ME1397)***, submitted to the National Institute of Technology, Rourkela for the award of Master of Technology in **Mechanical Engineering** with the specialization of "***Machine Design & Analysis",*** *is a record of bonafide research work carried out by him in the* ***Department of Mechanical Engineering,*** *under my supervision and guidance. I believe that this thesis fulfils part of the requirements for the award of the degree of Master of Technology. The results embodied in this thesis have not been submitted for the award of any other degree elsewhere.*

Dr. (Prof.) J. Srinivas
Dept. of Mechanical Engineering
National Institute of Technology,
Rourkela-769008, Odisha,
India.

Place: Rourkela
Date:

ACKNOWLEDGEMENT

I wish to express my deep sense of gratitude to **Dr. J. Srinivas, Professor,** Mechanical Engineering Department, for his wholehearted co-operation, unfailing inspiration and valuable guidance.

It is a privilege to express my deepest gratitude to **Dr. S. K. Sarangi,** Director and Professor **Dr. S.S. Mahapatra,** the Head of Department for extending the utmost support and cooperation to provide all the provisions & facilities for the successful completion of the project. I am extremely grateful to Mr. Prabhu Lakshmanan for his untimely support and his encouragement. I also wish to thank Ms Varalakshmi, Satish Teli & Ashish Gurjar for their suggestions throughout the project and their helpful company.

I also sincerely thank, the supporting staff for their sustained help in the successful completion of my project and all those who contributed directly or indirectly in successfully carrying out this work.

V. VISWA TEJA

Rourkela, May 2015

ABSTRACT

Wind turbine blade is one of the important components requiring more attention at the design stage. These blades are made up of fibrous material and sometimes hollow composite web sections may be employed in its construction. The main focus in its design is to achieve a desired strength to withstand various loads as per the power requirements. In view of this, modelling & dynamic analysis of blades is an essential requirement not only to avoid resonant vibrations but also to understand the stability of operation during various operating conditions. In this line, present work focuses on dynamics of horizontal- axis wind turbine blade with NACA 63415 profiles subjected to aerodynamic, centrifugal and gravity loads. The basic geometrical parameters of the blade are designed by using blade element moment method & the blade is modelled as a ruled 3D surface. By computing element wise cross sectional details from 3D model, a 1D beam finite element modelling is developed and modal characteristics are obtained. These are further validated with 3D finite element model result. Then, the effects of the tip speed ratio and rotational speed on the natural frequencies are studied. Further, finite element model have 10 elements with 6 degrees of freedom per node is used to obtain the dynamic response of the blade subjected to various loading conditions. The effect of aerodynamic, centrifugal and gravity parameters on the frequency response, edge-wise and flap-wise beating at the tip of blade are studied. The iterative programs developed in the work helps in testing the blade frequencies & response at any operating conditions. In order to estimate the stability during rotation, the frequency responses are obtained from response histories at the blade tip, by using Fast Fourier Transform algorithm. It is found that the centrifugal loads have profound effect on the frequency responses compared with other loads. The dynamics of long blade when rotating at varying wind conditions (aerodynamic loads) is influenced by gravity loads also.

INDEX

NOMENCLATURE

A_e	Area of Blade Element
a	axial induction factor
a’	angular induction factor
B	Number of blades
C_L	lift coefficient
C_D	drag coeffient
c	aerofoil chord length
C_p	Power Coefficient
dF_t	Thrust force
dF_d	Drag force
dM	Pitching Moment
I_e	Moment of Inertia of Blade element
N	Number of Blade elements
λ	Tip speed ratio
λ_r	local tip speed ratio
Ω	blade rotational speed
φ_s	setting angle
σ’	Local Solidity
ρ	density of the Glass fiber reinforced plastic material
ρ_a	density of the air at 15°C standard conditions

LIST OF FIGURES

LIST OF TABLES

Chapter-1

Introduction

Wind turbines can be classified into Horizontal Axis Wind Turbines (HAWT), and Vertical Axis Wind Turbines (VAWT). Horizontal type turbines have the blades rotating in a plane which is perpendicular to the axis of rotation. The HAWTs are most widely used type of wind turbines and come in varied sizes and shapes. The primary type of force acting on the blades of HAWT are the drag forces. The Horizontal type are commercially applicable type due to its varied sizes and storage capacities. In Vertical Axis Wind Turbine blades, the rotation axis coincides with the axis of generation of power. Advantages of Vertical Axis wind turbine is the placement of generator at the base of the turbine. But these type are nearer to ground which makes it difficult to capture the power at higher altitudes. While the HAWTs require yaw mechanism to orient themselves in the direction of wind, the VAWTs do not have such problem. But disadvantage with VAWTs is the low starting torque, lesser installation height and dynamic stability issues.

Any Horizontal axis wind turbine contains five major components: Rotor Blades, Rotor Hub, Nacelle, Yaw system and Tower. It is the shape of Blade which decides the tapping of wind energy and conversion into Kinetic energy of the blades. These blades have in general aerodynamic profiles and are constructed with materials having high strength to weight ratio. The tip speed ratio, number of blades and profile of the blades create huge difference in generation of wind power. The hub connects the rotor blades with the generator shaft. The nacelle houses a gearbox and generator to tap the power obtained at the shaft into electrical energy. A yaw mechanism is provided to the HAWT in order to orient itself to the wind direction. The sensitivity of the yaw mechanism plays important role in making the blade orient

itself towards the wind and improving efficiency of the turbine. The Tower provides the necessary altitude for the blades to overcome the obstacles that might cause turbulence in wind at smaller heights.

1.1 Wind Turbine Blades

Horizontal axis wind turbine blades are subjected to various type of excitations. Wind turbine blades has an aerofoil cross section with taper & twist incorporated to generate more output energy. During the rotation, the blade is subjected to centrifugal forces, and other aerodynamic effects as well as the gyroscopic coupling effect. Several earlier works studied these dynamic analysis problems of wind turbine blades. The modelling of the blade is carried out as a cantilever beam with unsymmetrical and variable cross section. Routine approach for study of such blades is finite element modelling where the beam is discretized into several elements, each having a defined area and Moment of Inertia. In practice for a lengthy wind turbine blade of unsymmetrical section, the element stiffness & mass matrices contain in total four Moments of Inertia, I_{xx}, I_{yy}, I_{zz} & I_{yz}.

Airfoils are common profiles for wind turbine blades. The blade contour must utilize the aerodynamic considerations while the material provides the stiffness and strength to the blade.

An airfoil is defined by a number of terms as shown in Figure 1.1. The leading edge is where the wind starts to hit the airfoil and trailing edge is where the air leaves the airfoil surface. The upper surface and lower surface of airfoil have a mean camber line midway between the two lines. The chord line connects the leading edge and trailing edge and the distance is designated by c. Camber is the maximum distance between the chord line and mean camber line. The angle of attack α is the angle at which the wind strikes the airfoil with relative wind velocity V_{rel}. The thickness of the airfoil is distance between the upper & lower surface of the airfoil. The chord length, thickness and camber affect the aerodynamic performance of the airfoil.

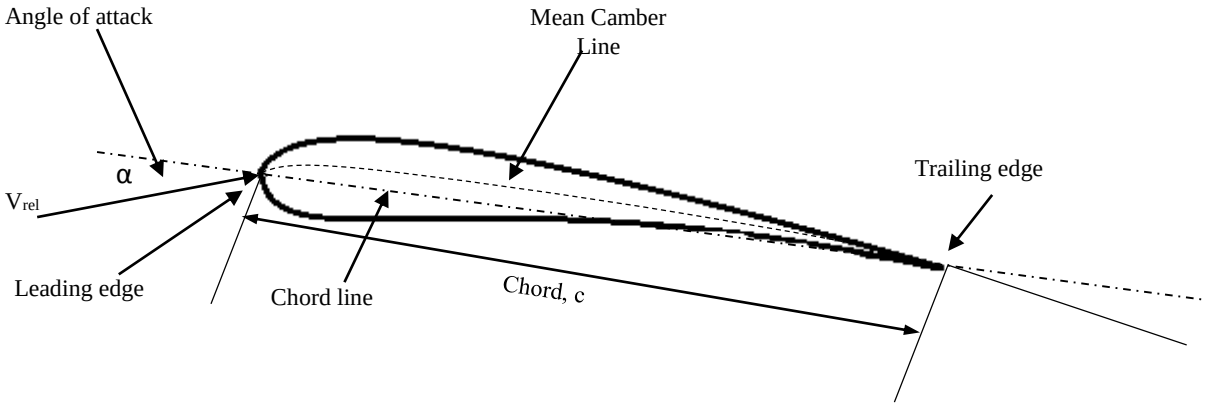

Fig 1.1 Airfoil profile Nomenclature

There are three widely wind turbine profiles which are NACA, LS & LM profile standards. Out of these, NACA airfoils have been widely accepted even in commercial applications due to their high power coefficients and lesser drag profiles. NACA stands for "*National Advisory Committee for Aeronautics".* In Horizontal axis wind turbines, the NACA profiles are used to generate the profile shape of the cross section of the blade by using a set of camber line equations to generate points on the upper and lower surface of the airfoil. The Shape of NACA airfoil is to be decoded from a series of digits which when substituted in the Equations gives the coordinates of the airfoil. There are different NACA series available for various aerospace, wind energy, rocketry applications out of which NACA 4 digit series and NACA 6 digit series provide better performance when used for generation of wind power.

1.2 Literature Review

In the area of wind turbine blade design and analysis several works are available in literature. These are summarized in this section.

Aerodynamic Design & Blade Optimization of Wind Turbine Blades:

Designing a blade by using well known Blade Element Momentum (BEM) Theory is a fascination to many researchers who are interested to get better geometrical parameters to maximize the power output of the blades.

National Advisory Committee for Aeronautics (NACA) developed a series of standard airfoil shapes which are prominent in usage as the profiles of the blades. Using the airfoil profile, knowing the angle of attack of the wind and the proposed length of the blade, researchers such as Tenguria et al. [1] have used BEM theory to optimize the coefficient of power, lift and drag characteristics with various tip speed ratio, lift and drag coefficients. It is observed that at a power coefficient 0.46 and lift to drag coefficient is 124.47, the power absorption is maximum.

John McCosker [2], developed an optimized code for a discretized 9 element wind turbine blade having a length of 0.95 m. He obtained optimal speed ratio, angle of wind, the pitch angle and relative chord lengths for each element. After convergence, the power extracted from wind is found to be 0.81 KW. The airfoil shape is varied from NACA 4412 to NACA 23012 where the angle of attack of the blade to get maximum glide ratio is found different for each profile.

Cost reduction of generation of wind power is critical and it can be possible by suitable structural design changes and use of composite materials to lead greater profits. This is discussed by Anjali et al [3], in which they described an ant colony optimization method by varying the composite material of the blade and conducting stress analysis. Ultimately, he

obtained the optimized values of chord length and blade twist angles and it is found that Kevlar 149 material has highest natural frequency and less deflection compared to others.

Thumthae and Chitsomboon [4] investigated an untwisted blade for obtaining optimal pitch to get maximum power for wind turbine using stead flow wind conditions. Research is also done using Genetic algorithms to obtain the optimization of chord and twist angle by Juan Mendez and Greiner [5], for a test turbine having 19m rotor diameter and 100 KW nominal power. Similar works have been done [6-9] where observations state that optimizing the blade shape parameters is mostly to maximize the output power generation of the blade.

Ingram [8] derived equations relating to the Blade Element Theory in order to find the axial force, Lift and drag characteristics, considering the tip loss correction to calculate the rotor performance. An iterative procedure is used to refine the obtained results.

Vasjaliya et al [9], evaluated multidisciplinary optimization process to minimize cost, weight and maximize power output by considering a fluid structure interaction and structural robustness to enhance performance of a QBlade / XFoil airfoil blade. In process of optimization, structure and design variables are taken as input parameters and a number of DOEs were created and solved.

Sedaghat et al. [10] used BEM Theory to get a generalized quadratic equation on angular induction factor with tip speed ratio, drag to lift coefficient. Then an optimal blade geometry is obtained which is used to calculate the power performance at variable speeds. BEM theory ensures quicker way to understand the off design power performance of blades moving at a constant speed.

Using 3D modelling softwares such as CATIA, Solidworks, the design of wind turbine blade can be seen much more realistically. These surface models can even be exported to analysis

packages to conduct further research analysis by posing suitable conditions. Scott Larwood et al. [11] studied the design of a swept wind turbine blade. Parametric study to determine sweep parameters using STAR7d scaled model showed that loads were most sensitive on the tip of sweep.

Finite Element Analysis & Modal Analysis of Wind Turbine Blades:

Today, the method of finding the modes of vibration of a structure has become widespread to assess the inherent properties of the structure. The significance of finding the solution for these single degree of freedom systems is such that they can be used to analyse the complex multiple degree of freedom systems as the latter can be decoupled into a system of Single degree of freedom systems. [12-16] discusses the experimental and numerical investigations done on performing Modal Analysis on complex wind turbine blades.

Gursel et al. [12] studied the vibration characteristics of rotor blades using approximation method such as Rayleigh to calculate the natural frequency of each blade. They have validated the results of vibration analysis by using Finite element analysis.

Larsen et al. [13] shown experiments on a LM 19m blade to investigate the mode shapes, dominating deflections, and explained the difference or error in measurement between the theoretically computed values and experimental results. It is observed that for non – dominating deflection direction, the measured and computed mode shapes are found to be in good agreement. A forced vibration damper is introduced in the experimental setup to check the damping characteristics of the blade.

Liu et al [14] studied modal and harmonic analysis of circumferential force is on a 5MW S809 airfoil, wind turbine model to obtain the natural vibration characteristics to get first seven orders of natural frequencies along with harmonic responses in different phases.

Allikas et al. [15] validated a full scale single layer layup small horizontal axis wind turbine blade through experimental bending test and modal analysis. They have taken Glass fiber reinforced composite plastics to get the stiffness and strength analysis acted by 7848 N load. A difference if 16.8% occurred during load Case 6, damaging the blade due to value of obtained stress being greater than yield strength of the skin element of blade.

Sami et al. [16] extracted fundamental flapwise and edgewise modal frequency of a 5KW GFRP wind turbine blade by using 3d shell elements. It is to understand better the dynamic behaviour that he conducted experiments using electrodynamic shaker system to predict the resonant frequencies. He observed that flapwise frequencies are found to be in agreement to each other while % of error is more in case of edgewise frequency.

Fangfang song [17] worked on optimization of design of the blade, having NACA 63415 profile and then modelled the surface model of blade using Solidworks software. Then the finite element model is considered to find out the modal analysis of the blade. The excited frequeny from wind speed of 10m/s is calculated as 7.16 Hz which is found to be more than the fundamental frequency obtained from the modal analysis therefore no resonance will occur when the blades run at rated wind speed.

Dynamic Analysis:

Jie et al [18], used a 38m blade having rated power 1500KW and conducted structural stress and strain distribution analysis to understand the flapwise loads and vibration mode shapes. Shell 99 elements are used to discretize the blade using Finite Element Analysis to validate the result. The authors have conducted structural response characteristics [19] to study the aerodynamic characteristics using CFD simulation and then formulating dynamic characteristics of the blade. The BEM method predicted much higher aerodynamic loads than

CFD method. A maximum error of 4.86% is observed between FE model and calculated frequencies.

Inoue et al. [20] studied the dynamic analysis of wind turbine blade by investigating its fundamental vibration behaviour. Effect of gravitational and wind load on super harmonic resonance was presented.

Lag wise dynamic characteristics of a wind turbine blade subjected to unsteady aerodynamic forces was studied by Li et al. [21]. A mathematical model [22] is developed for describing non-linear vibration of horizontal axis wind turbines which uses Kelvin Voigt Theory to compute the decouple a set of coupled equations of motion representing a wind turbine blade subjected to aerodynamic and gravitational loads. The expressions for static deformation, aero elastic stability and dynamics of the blade are solved from the set of equations. The system consists of a rotating blade with out of plane bending having in plane bend and torsion. Factors such as coning angle, twist angle, eccentricity, mass centre, shear centre were included.

Li et al. [23] also conducted the dynamic response analysis for flap wise direction in case of super harmonic response. Amplitude modulation equations are used to derive frequency response. Effect of static displacement, perturbation frequency, dynamic displacements are studied and results are compared with numerical solution. It is found that dynamic displacements of flap wise are larger compared to axial displacements of the blade.

Hamdi et al. [24] independently presented forced vibration analysis of wind turbine blade rotating at a constant angular velocity by taking into consideration aerodynamic, centrifugal, gravity and gyroscopic loads. In this, both static and dynamic investigation studies have been discussed with and without gyroscopic loads is done. The excitation force vector containing harmonic components is incorporated in the equations of motion, and the differential equations

are solved by using Newmark method. Dynamic responses along with FFT responses are obtained for blade for the first 25 seconds.

Karadag [25] studied effect of shear center on dynamic characteristics of the blade. Different methods such as Reissner, Potential and finite element methods are used to calculate the natural frequencies of the blade rotating at 0 rpm and 3500 rpm for the loads acting at the shear centres. The bending and torsional modes are observed and variation is found for finite element method and Reissner method. It is seen that shear center affects the natural frequencies and modes of the rotating beams with complex geometry. Both thick beam and thin beam theories give results in close comparison. Torsional frequencies show greater change with increase of rotation than the bending frequencies.

Nymann et al. [26] described a formulation of 3D two node FE analysis in rotating frame of reference. The effect of Elastic, geometric and torsional bending are shown to play significant role in improving accuracy modelling of structures. Structural responses at middle of the blade and blade tip is observed. The actuator forces seem to reduce material strains at all times.

Keerthana et al. [27] introduced a step wise procedure to develop the blade's geometrical properties by using optimization techniques and taking input parameters as the tip speed ratio, wind speed and the aerofoil properties, the chord, twist distributions are calculated. Then a CFD analysis for obtaining the lift & drag coefficients (C_L and C_D) is done to calculate the lift and drag forces acting on the blade.

Yangfeng Wang [28] considered two cases of turbine blades having 1m and 5m in length and conducted damage detection technique by comparing the dynamic response analysis and mode shape curvature methods using composite multi-layer materials. The dynamic analysis method is used to understand the damage severity of wind turbine blades.

Chu and Clausen [29] used 5KW horizontal axis wind turbine blade 2.5m long to find out the dynamic response using LXRS telemetry system which uses 3 gauges to measure the response during operation. At small speeds, turbine operation is satisfactory, but yaw error is found to increase as speed increased to large extent. Zheng et al. [30] found dynamic response by considering flexible beam elements and obtained the response characteristics for a medium and high speed wind turbine.

1.3 Scope and Objectives

Most of the literature dealt with investigation of various airfoils design, aerodynamic evaluation by simulation tools, and the analysis of complex composite web section blades using various techniques including FE modelling, analytical approaches as well as experimental works. Very few works considered the power generation by blades of around 1m length for analysis. There is a requirement of developing a user interactive software that computes the blade data corresponding to flow conditions and generate the dynamic response using some finite element approach.

In the present work, research is carried out with inclusion of the following aspects: Performance of wind turbine blade models with NACA 63415 profile, airfoil blade section analysis with taper and twist, in stationary and rotating conditions, modal data & forced vibration analysis, using analytical and FE Modelling.

Initially, a dynamic model of the wind turbine blade is carried using Finite element modelling. The blade design parameters are found out by using the Blade Element Momentum theory which defines the geometry of the blade. A computer aided design model of the blade is developed in CATIA software with wind turbine blade having lengths of 1.02 m of NACA 63415 airfoil. The model is analysed in ANSYS and the frequency (modal) data is obtained. Further, dynamic analysis of the blades is carried out using beam finite elements and the nodal

forces are applied including aerodynamic lift & drag forces, centrifugal forces and gravity loads.

1.4 Thesis Organization

The remaining thesis is organized as follows: Chapter 2 explains the dynamic equations of motion for out of plane bending vibrations of a rotating tapered twisted wind turbine blade, the BEM method and types of loading a wind turbine blade is generally subjected to. Chapter 3 introduces finite element modelling on the blade by applying centrifugal, aerodynamic, and gyroscopic loads on the blade element. The results and discussion of the modal and dynamic analysis are presented in Chapter 4. In Chapter 5, conclusions are made and future scope of the work is illustrated.

Chapter-2

Mathematical Modelling

2.1 Equations of Motion of a Rotating Wind Turbine Blade

Due to high slenderness ratio, often the wind-turbine blade is treated as a rotating Euler-Bernoulli beam. Let a blade of length L is mounted on the hub of radius R at a settling angle φ_s and with an inclination angle θ as shown in Fig 2.1.

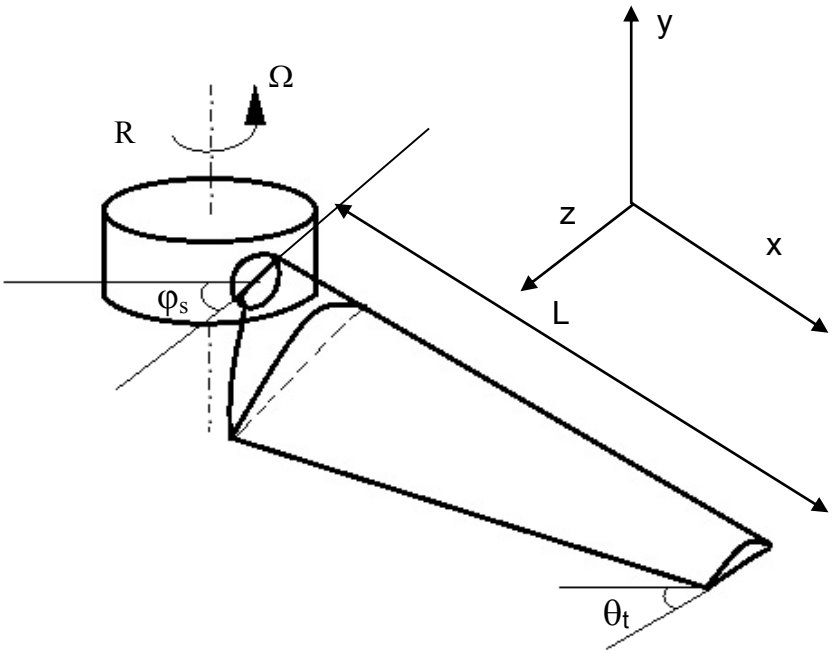

Fig 2.1 Blade configuration

Also, if Ω is constant angular speed, then any point on the deformed blade can be expressed as:

$$\vec{OP} = \begin{Bmatrix} R + (x+u)\cos\theta_t - v\sin\theta_t \sin\varphi_s \\ (x+u)\sin\theta_t + v\cos\theta_t \sin\varphi_s \\ v\cos\varphi_s \end{Bmatrix} \tag{2.1}$$

The kinetic and potential energies of the system are given by:

$$T=\frac{1}{2}\int_0^L\int_A \rho(\vec{V}_p..\vec{V}_p)dAdx \tag{2.2}$$

$$U=\frac{1}{2}\int_0^L\int_A E\varepsilon_x{}^2 dAdx \tag{2.3}$$

Where, ρ and E are density and elastic modulus of material, while ε_x is normal strain given in terms of displacements as follows

$$\varepsilon_x=\frac{\partial u}{\partial x}-r\frac{\partial^2 v}{\partial x^2}+\frac{1}{2}\left(\frac{\partial v}{\partial x}\right)^2 \tag{2.4}$$

Here, r is the distance of arbitrary point to the centroidal axis. The non-conservative virtual work done by aerodynamic forces and moments is given by:

$$\delta W = F_x\delta x + F_y\delta y + M_z\delta y' \tag{2.5}$$

The Governing partial differential equation of motion of such a beam in flap wise bending mode can be shown as:

$$\begin{aligned}&\frac{\partial^2}{\partial x^2}\left[EI(x)\frac{\partial^2}{\partial x^2}\left(y(x,t)\right)\right]+\rho A(x)\frac{\partial^2 y(x,t)}{\partial t^2}-\left[\int_x^l f_{cent}(\xi,t)d\xi\right]\frac{\partial^2 y(x,t)}{\partial x^2}\\&+f_{cent}(x,t).\frac{\partial y(x,t)}{\partial x}=0\end{aligned} \tag{2.6}$$

Where, f_{cent} is the centrifugal force acting on the blade given by,

$$f_{cent}=\rho\Omega^2 A(x)(r+x) \tag{2.7}$$

and ρ is the density, l is the length of beam, and ξ is dummy variable for x.

By substituting f_{cent}, we get:

$$\begin{aligned}&EI(x)(y^{IV}+\eta\dot{y}^{IV})+2EI'(x)(y'''+\eta\dot{y}''')+EI''(x)(y''+\eta\dot{y}'')+\rho A(x)y\\&-\rho\Omega^2\left[\left(\int_x^l A(\xi)(r+\xi)d\xi\right)y''-A(x)(r+x)y'\right]=0\end{aligned} \tag{2.8}$$

Where dot represent differential with respect to time and primes denote differential with respect to x and A(x), I(x) are the cross section area and Polar Moment of inertia of blade element.

2.2 Approximate Solution approach

Galerkin's approach is used to solve the above set of equations by considering the k^{th} order estimate. By Galerkin's expansion, expression for y(x,t) changes to:

$$y(x,t) = \sum_{p=1}^{k} g_p(\tau)\varphi_p(x) \tag{2.9}$$

The boundary conditions for cantilever beam are

$$y(0) = 0, y'(0) = 0, y''(1) = 0, y'''(1) = 0 \tag{2.10}$$

where $\varphi_p(x)$ contains eigen functions of a stationary, Euler-Bernoulli beam satisfying the boundary conditions (2.10) and are written as:

$$\varphi_{p(x)} = \cosh\lambda_p x - \cos\lambda_p x - k_p(\sinh\lambda_p x - \sin\lambda_p x) \tag{2.11}$$

$$k_p = \frac{\cosh\lambda_p + \cos\lambda_i}{\sinh\lambda_p + \sin\lambda_p} \tag{2.12}$$

where, λ_p are the eigen frequencies which are the roots of the equation $1+\cos\lambda\cosh\lambda = 0$.

Substituting the value of Equation (2.10) into (2.8) gives the following expression:

$$\begin{aligned}&\mathrm{Re}\,s(y) = EI(x)g(t)\psi^{IV}(x) + 2EI'(x)g(t)\psi'''(x) + EI''g(t)\psi''(x) + \rho A(x)\ddot{g}(t)\psi(x)\\ &-\rho\Omega^2\left[\left(\int_{x=0}^{l} A(\xi)(r+\xi)d\xi\right)g(t)\psi''(x) - A(x)(r+x)g(t)\psi'(x)\right] = 0\end{aligned} \tag{2.13}$$

Orthogonalizing the residual with respect to the set of $\varphi_q(x)$, we obtain,

$$\int_0^l \mathrm{Re}\,s(y)\varphi_q(x)dx = 0 \text{ , q=1,2,3…,k} \tag{2.14}$$

As a procedure of Galerkin's method, the approximate discretized equations of motion for 1st eigen frequency of λ_p= 1.8751 are formed and the equations in time domain are solved and the final solution is obtained by multiplying it with mode shape function at any location x.

2.3 Loads Acting on Wind Turbine Blade

The wind turbine blade profiles are constructed by combining the concepts of 2-dimensional airfoil and Blade Element Momentum theory. The chord and twist distributions are obtained from BEM theory whereas as the profile can be constructed form the camber line equations shown in Appendix I. A lofted surface is modelled in a design software to obtain the 3-Dimensional realistic view of the model of blade. Blade Element Momentum Theory (BEM) discretizes the whole blade into a number of elements and couples the momentum theory with local forces acting on each blade element. The first method examines the momentum balance of a rotating turbine in a stream tube with wind passing over it. The second method determines the lift & drag forces. These two methods gives a series of equations to solve the blade element cross section as independent forces are assumed to be acting on each blade element. The model is based on Rankine Froude Momentum model which has the following assumptions: no aerodynamic interactions amongst blade elements, velocity in direction of length of blade is neglected, the forces are assumed to be dependent only on lift and drag coefficients.

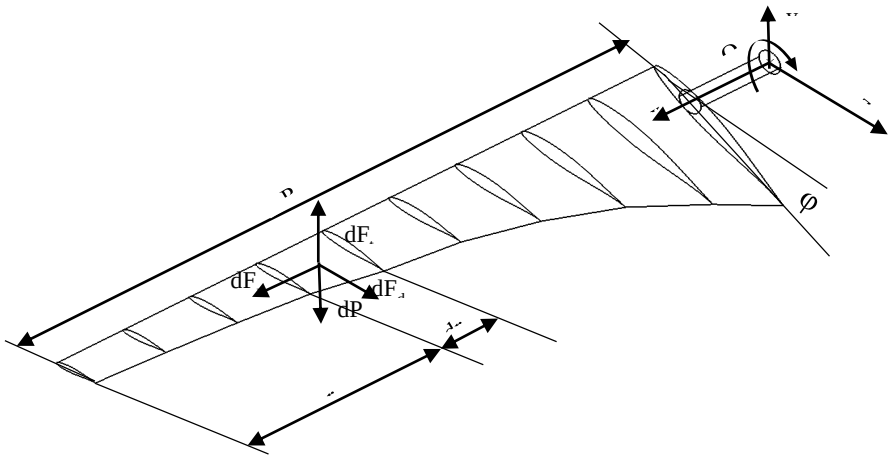

Fig 2.2 Representation of Blade elements and blade geometry

We cannot tap the entire energy available in the wind as only the wind which passing through the blades can be utilized in generation of power. For more power, require to have infinite number of blades rotating with negligible thickness. Since that cannot be possible, Betz investigated the maximum conversion efficiency and found that we can convert only 59.25% of available wind power into electricity. This is known as the Betz Limit and it determines the criterion we have to consider when thinking to design a wind turbine generating a specific power. So any wind turbine blade cannot have the value of Power Coefficient C_P more than 16/27. Wind turbine blade is subjected to a complex loading subjected to random wind loading. There are basically four major types of loading any wind turbine blade undergoes.

2.3.1 Aerodynamic Loads

These loads are based on the type of airfoil profile selected. These loads are applied due to flow of wind over the blade and are the primary loading which generates the power. The aerodynamic loads are of three types: Thrust Force dF_t, Drag Force dF_d and Pitching Moment dM. are represented in Figure 2.2.

1. ***Thrust Force (F_T)***: It acts on the lower surface of the blade in perpendicular direction as a result of the unequal pressure on the top and bottom surfaces of the blade.

$$\text{Thrust Force: } F_T = \frac{1}{2}\rho_a C_y c_e V^2 dx \tag{2.15}$$

2. ***Drag Force (F_D)***: This force acts in the plane of rotation opposite to rotation and it is due to visocity of the fluid making the blade to lower its speed.

$$\text{Drag Force: } F_D = \frac{1}{2}\rho_a C_z c_e V^2 dx \tag{2.16}$$

3. ***Pitching Moment (M_p):*** acts along direction of the span of the blade which causes torsion of blade.

$$\text{Moment } M_p = \frac{1}{2}\rho_a C_m c_e^2 V^2 dx \tag{2.17}$$

2.3.2 Centrifugal & Gravitational Loads:

These type of loads depend of the angular Rotational speed of the blade Ω, the mass of the blade and is expressed as:

$$F_{cent} = \sum_{x=0}^{x=l} \rho A \Omega^2 x dx \tag{2.18}$$

The gravitational load is simply given as

$$F_G = \sum_{e=1}^{n} m_e g v = m_{blade} g \tag{2.19}$$

2.3.3 Gyroscopic Load

The Gyroscopic loads causes a tilt moment to occur when the blade is rotating and simultaneously a yaw mechanism is installed for changing the blade's orientation with respect to the wind direction. This combined effect will produce a resulting yaw moment and tilt moment. But in 3 bladed turbines, the yaw moment is neglected and Tilt moment M_{tilt} is expressed as:

$$M_{tilt} = 3\omega\omega_k \sum_{e=1}^{n} m_e r_e^2 \tag{2.20}$$

Chapter-3

Finite Element Model of the blade

3.1 Blade Discretization

The taper-twisted wind turbine blade is discretized into n elements using BEM Theory where each element has length of l_e, a cross sectional area of A_e. A six degree of freedom two noded Euler beam element is considered with displacement vector $q_e = [u_i, v_i, w_i, \alpha_i, \beta_i, \gamma_i, u_j, v_j, w_j, \alpha_j, \beta_j, \gamma_j]^T$ where i and j denote the node numbers. Fig.3.1 shows the discretization of blade from root to tip.

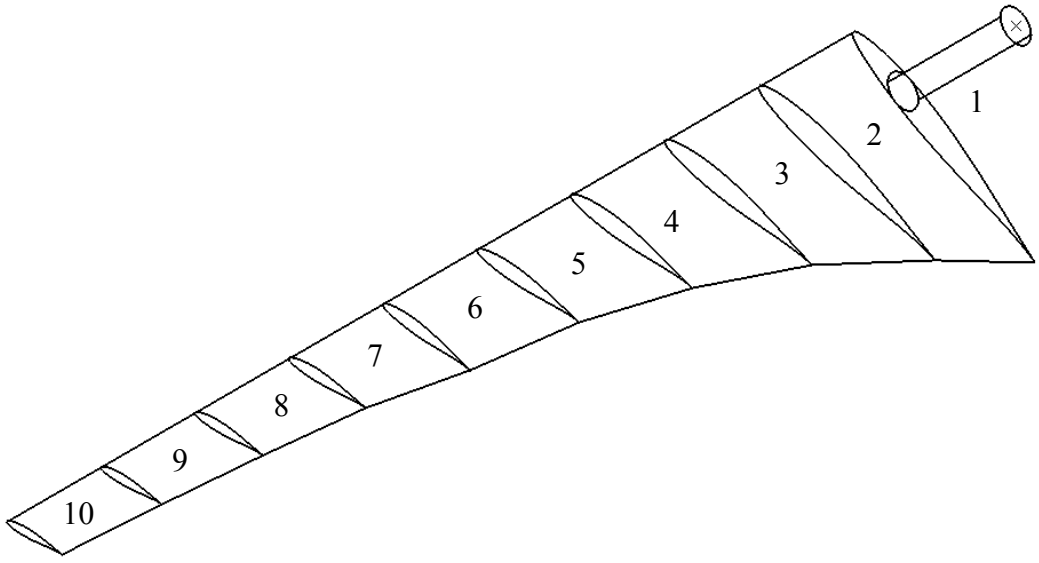

Fig 3.1 Discretization of the blade

The stiffness matrix of blade element **K** is calculated as:

$$[K]^e = \begin{bmatrix}
\frac{AE}{L} & 0 & 0 & 0 & 0 & 0 & \frac{-AE}{L} & 0 & 0 & 0 & 0 & 0 \\
0 & \frac{12EI_z}{L^3} & \frac{12EI_{yz}}{L^3} & 0 & \frac{-6EI_{yz}}{L^2} & \frac{6EI_z}{L^2} & 0 & \frac{-12EI_z}{L^3} & \frac{-12EI_{yz}}{L^3} & 0 & \frac{-6EI_{yz}}{L^2} & \frac{6EI_z}{L^2} \\
0 & \frac{12EI_{yz}}{L^3} & \frac{12EI_y}{L^3} & 0 & \frac{-6EI_y}{L^2} & \frac{6EI_{yz}}{L^2} & 0 & \frac{-12EI_{yz}}{L^3} & \frac{-12EI_y}{L^3} & 0 & \frac{-6EI_y}{L^2} & \frac{6EI_{yz}}{L^2} \\
0 & 0 & 0 & \frac{GJ_x}{L} & 0 & 0 & 0 & 0 & 0 & \frac{-GJ_x}{L} & 0 & 0 \\
0 & \frac{-6EI_{yz}}{L^2} & \frac{-6EI_y}{L^2} & 0 & \frac{4EI_y}{L} & \frac{-4EI_{yz}}{L} & 0 & \frac{6EI_{yz}}{L^2} & \frac{6EI_y}{L^2} & 0 & \frac{2EI_y}{L} & \frac{-2EI_{yz}}{L} \\
0 & \frac{6EI_z}{L^2} & \frac{6EI_{yz}}{L^2} & 0 & \frac{-4EI_{yz}}{L} & \frac{4EI_z}{L} & 0 & \frac{-6EI_z}{L^2} & \frac{-6EI_{yz}}{L^2} & 0 & \frac{-2EI_{yz}}{L} & \frac{2EI_z}{L} \\
\frac{-AE}{L} & 0 & 0 & 0 & 0 & 0 & \frac{AE}{L} & 0 & 0 & 0 & 0 & 0 \\
0 & \frac{-12EI_z}{L^3} & \frac{-12EI_{yz}}{L^3} & 0 & \frac{6EI_{yz}}{L^2} & \frac{-6EI_z}{L^2} & 0 & \frac{12EI_z}{L^3} & \frac{12EI_{yz}}{L^3} & 0 & \frac{6EI_{yz}}{L^2} & \frac{-6EI_z}{L^2} \\
0 & \frac{-12EI_{yz}}{L^3} & \frac{-12EI_y}{L^3} & 0 & \frac{6EI_y}{L^2} & \frac{-6EI_{yz}}{L^2} & 0 & \frac{12EI_{yz}}{L^3} & \frac{12EI_y}{L^3} & 0 & \frac{6EI_y}{L^2} & \frac{-6EI_{yz}}{L^2} \\
0 & 0 & 0 & \frac{-GJ_x}{L} & 0 & 0 & 0 & 0 & 0 & \frac{GJ_x}{L} & 0 & 0 \\
0 & \frac{-6EI_{yz}}{L^2} & \frac{-6EI_y}{L^2} & 0 & \frac{2EI_y}{L} & \frac{-2EI_{yz}}{L} & 0 & \frac{6EI_{yz}}{L^2} & \frac{6EI_y}{L^2} & 0 & \frac{4EI_y}{L} & \frac{-4EI_{yz}}{L} \\
0 & \frac{6EI_z}{L^2} & \frac{6EI_{yz}}{L^2} & 0 & \frac{-2EI_{yz}}{L} & \frac{2EI_z}{L} & 0 & \frac{-6EI_z}{L^2} & \frac{-6EI_{yz}}{L^2} & 0 & \frac{-4EI_{yz}}{L} & \frac{4EI_z}{L}
\end{bmatrix} \quad (3.1)$$

Euler configuration is applied to each blade element to develop the equation of Kinetic energy of blade elements. From kinetic energy of the system, the expression for element mass matrix is given by:

$$[M]^e = \rho A_e l_e \begin{bmatrix}
\frac{1}{3} & 0 & 0 & 0 & 0 & 0 & \frac{1}{6} & 0 & 0 & 0 & 0 & 0 \\
0 & \frac{13}{35} & 0 & 0 & 0 & \frac{11L}{210} & 0 & \frac{9}{70} & 0 & 0 & 0 & \frac{-13L}{420} \\
0 & 0 & \frac{13}{35} & 0 & \frac{-11L}{210} & 0 & 0 & 0 & \frac{9}{70} & 0 & \frac{13L}{420} & 0 \\
0 & 0 & 0 & \frac{I_y + I_z}{3A} & 0 & 0 & 0 & 0 & 0 & \frac{I_y + I_z}{6A} & 0 & 0 \\
0 & 0 & \frac{-11L}{210} & 0 & \frac{L^2}{105} & 0 & 0 & 0 & \frac{-13L}{420} & 0 & \frac{-L^2}{140} & 0 \\
0 & \frac{11L}{210} & 0 & 0 & 0 & \frac{L^2}{105} & 0 & \frac{13L}{420} & 0 & 0 & 0 & \frac{-L^2}{140} \\
\frac{1}{6} & 0 & 0 & 0 & 0 & 0 & \frac{1}{3} & 0 & 0 & 0 & 0 & 0 \\
0 & \frac{9}{70} & 0 & 0 & 0 & \frac{13L}{420} & 0 & \frac{13}{35} & 0 & 0 & 0 & \frac{-11L}{210} \\
0 & 0 & \frac{9}{70} & 0 & \frac{-13L}{420} & 0 & 0 & 0 & \frac{13}{35} & 0 & \frac{11L}{210} & 0 \\
0 & 0 & 0 & \frac{I_y + I_z}{6A} & 0 & 0 & 0 & 0 & 0 & \frac{I_y + I_z}{3A} & 0 & 0 \\
0 & 0 & \frac{13L}{420} & 0 & \frac{-L^2}{140} & 0 & 0 & 0 & \frac{11L}{210} & 0 & \frac{L^2}{105} & 0 \\
0 & \frac{13L}{420} & 0 & 0 & 0 & \frac{-L^2}{140} & 0 & \frac{-11L}{210} & 0 & 0 & 0 & \frac{L^2}{105}
\end{bmatrix} \quad (3.2)$$

Henceforth, the linear equation system becomes

$$M_e\ddot{X}_e + C_e\dot{X}_e + K_eX_e = F_e \tag{3.3}$$

Where C_e is internal damping matrix of the system, F_e is the generalized force vector which contains aerodynamic, centrifugal, gravity, and gyroscopic loads which are computed using Blade Element Momentum theory (BEM) in case of an isothermal flow of a viscous and incompressible fluid. The expressions for thrust force dF_t, drag force dF_d and pitching moment dM are given in chapter 2 and complete element force vector is defined below.

$$\begin{aligned} dF_t &= \frac{1}{2}\rho_a C_y c_e V_r^2 dx \\ dF_d &= \frac{1}{2}\rho_a C_z c_e V_r^2 dx \\ dM &= \frac{1}{2}\rho_a C_m c_e^2 V_r^2 dx \end{aligned} \tag{3.4}$$

Where C_x, C_y, and C_m are the lift, drag and moment coefficients respectively and are given by:

$$\begin{aligned} C_y &= C_L \sin\phi_r + C_D \cos\phi_r \\ C_z &= C_D \sin\phi_r - C_L \cos\phi_r \end{aligned} \tag{3.5}$$

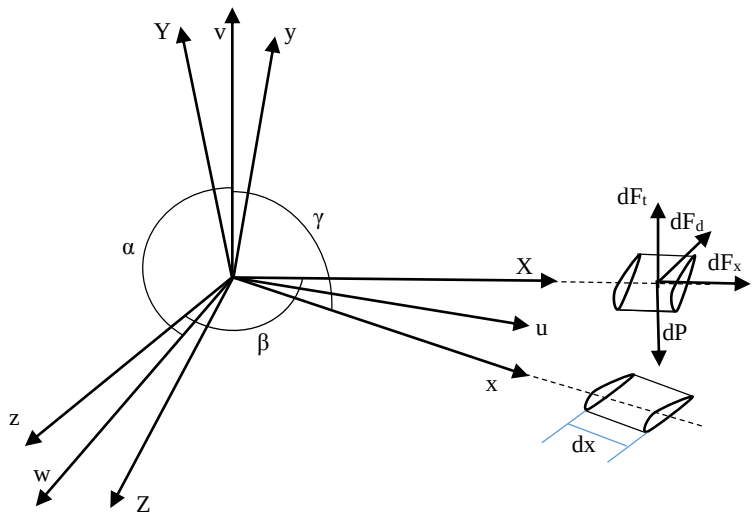

Fig 3.2 Euler configuration of the blade

Similarly, the Centrifugal force and the gravity load vector acting on each blade element of length dx (see Fig.3.2) in terms of elemental cross sectional area A_e given by:

$$dF_{cent} = \rho A_e \Omega^2 dx \tag{3.6}$$

$$dP = -\rho g A_e \left[\cos\delta \sin\Omega t, \cos\delta \cos\Omega t, \sin\delta\right]^T dx \tag{3.7}$$

The total elementary force vector dF_e is simplified as:

$$dF_e = \begin{bmatrix} \frac{1}{2}\rho l\Omega^2 A_e\left(2x_i + x_j\right) - \frac{1}{2}\rho g l A_e \cos\delta \sin\Omega t \\ \frac{1}{4}\rho_a l C_y c_e V_r^2 - \frac{1}{2}\rho g l A_e \cos\delta \cos\Omega t \\ \frac{1}{4}\rho_a l C_z c_e V_r^2 - \frac{1}{2}\rho g l A_e \sin\delta \\ \frac{1}{4}\rho_a l C_m {c_e}^2 V_r^2 - \frac{1}{2}\rho l\Omega^2 I_{yz} \\ 0 \\ 0 \\ \frac{1}{2}\rho l\Omega^2 A_e\left(2x_j + x_i\right) - \frac{1}{2}\rho g l A_e \cos\delta \sin\Omega t \\ \frac{1}{4}\rho_a l C_y c_e V_r^2 - \frac{1}{2}\rho g l A_e \cos\delta \cos\Omega t \\ \frac{1}{4}\rho_a l C_z c_e V_r^2 - \frac{1}{2}\rho g l A_e \sin\delta \\ \frac{1}{4}\rho_a l C_m {c_e}^2 V_r^2 - \frac{1}{2}\rho l\Omega^2 I_{yz} \\ 0 \\ 0 \end{bmatrix} \tag{3.8}$$

The resultant solution will contain a number of ordinary differential equation. A numerical time integration method such as Newmark method is to be employed to solve for the dynamic responses. The steps of this method are given in Appendix III.

3.2 3D Modelling of the Blade

The values of coordinates of top and bottom surfaces of airfoil as stored in excel format are called in commercial solid model software CATIA V5. The macro after pasting the coordinates prompts an option either to generate only points, or points & spline, or loft the splines. The inserted spline in the CATIA part file is either scaled to the required size or rotated to give the

amount of twist to the wind turbine blade. After getting the two splines, the surface modelling feature is activated and a loft surface is formed by multi section solids option from CATIA toolbox. After getting the loft surfaces, upper and lower surfaces are joined so that we get a solid model ready for analysis as shown in Fig.3.3. The solid model obtained is saved in either .parasolid or .igs format and is exported to ANSYS for further analysis as seen in Fig.3.4. The first few natural frequencies of the system can be found out using ANSYS workbench which will serve as a base for transient and vibrational analysis of the system. In this analysis, the wind turbine blade is simplified to be a cantilever problem where the blade is fixed at the hub portion.

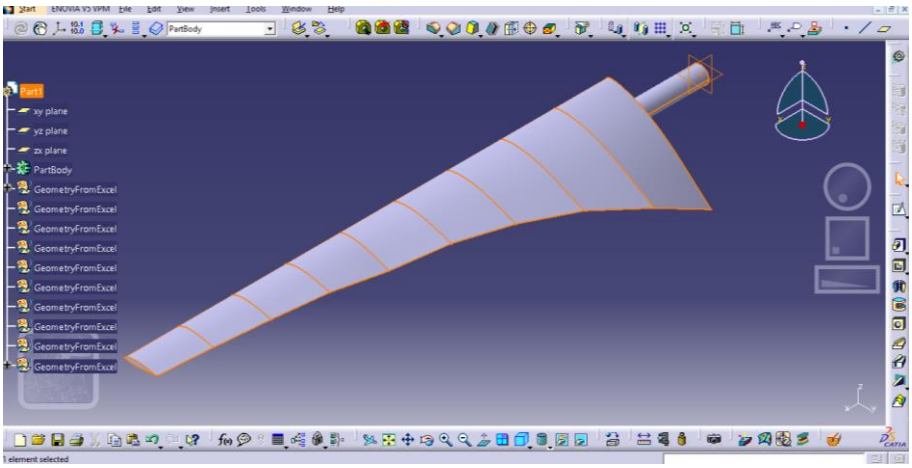

Fig 3.3 Solid model of the twisted blade

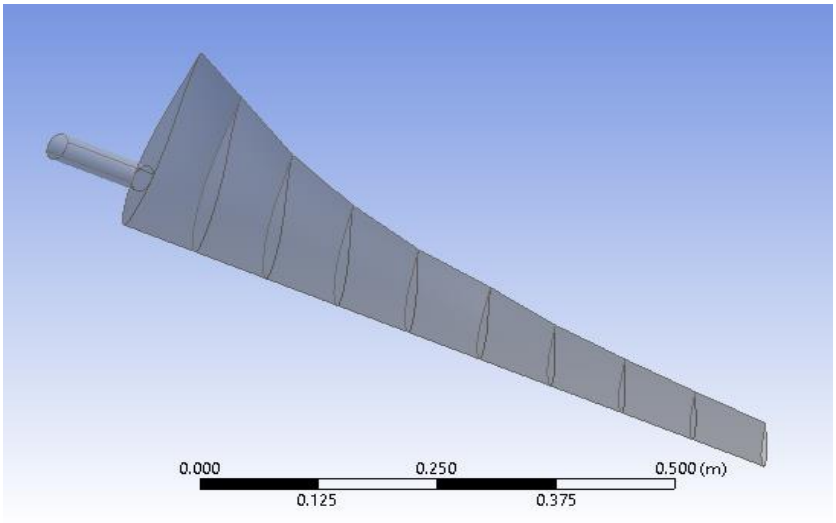

Fig 3.4 Imported solid model

The .igs file is opened in ANSYS workbench for modal analysis. The modal analysis tool is invoked, the materials are given and the geometry is imported into the workbench. The total deformation and first five natural frequencies are obtained and their mode shapes are recorded.

Chapter-4

Results & Discussion

Dynamic analysis of such coupled fluid-structure problem required several considerations. First step is to generate the blade geometry. Then CAD model is formulated in 3-D, followed by its frequency analysis. 1-D beam formulation is then presented with the generated force system. The dynamic equations are solved by Newmark's time integration with zero initial conditions. Details are explained one after the other as follows.

4.1 Blade Data Selection Procedure

An important factor to consider in generation of power of wind turbine is the blade design. The following procedure is to be adopted in determining the blade dimensional properties.

Step 1: Determine the radius of the blade **R = 1.02m**

Step 2: Choose a tip speed ratio **λ=6**

Step 3: The number of blades **B=3**

Step 4: Select an airfoil: **NACA 63415**

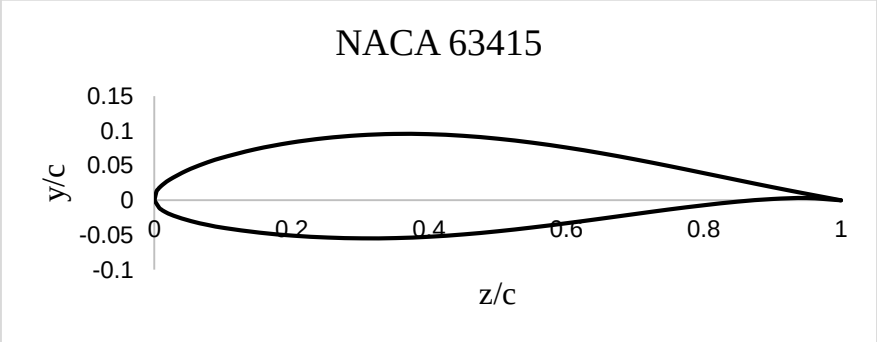

Fig 4.1 Aerodynamic profile of NACA 63-415 airfoil

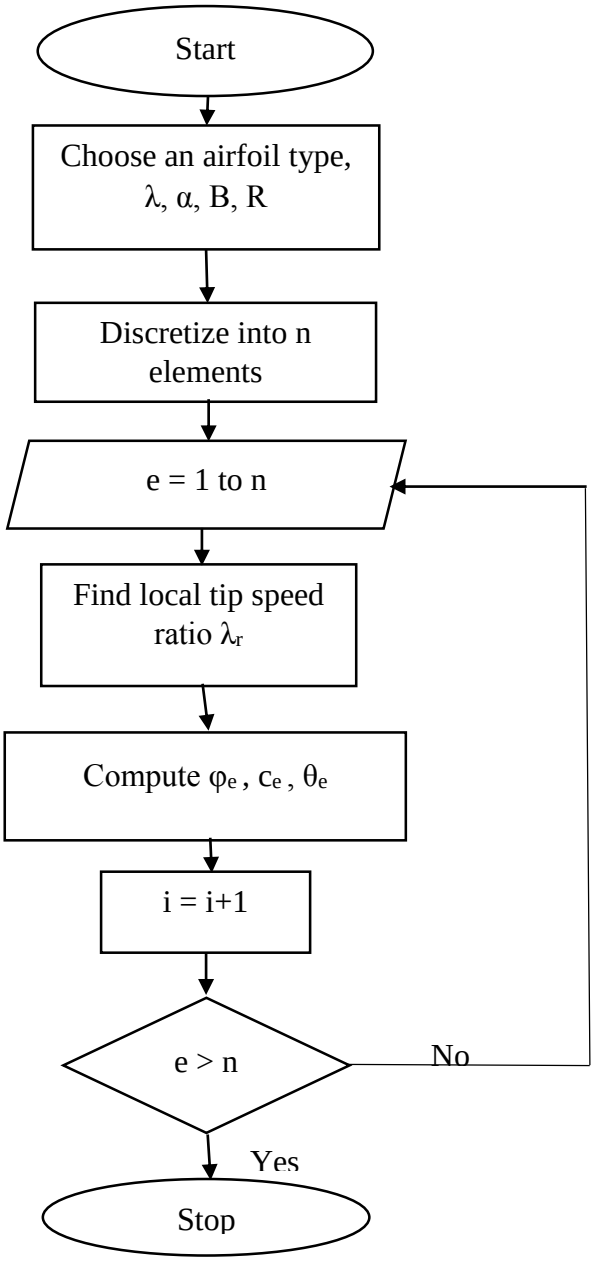

Fig 4.2 Flowchart to determine blade's geometric parameters

Step 5: Choose a chord distribution of the aerofoil

$$c = \frac{8\pi r}{BC_L}\left(1-\cos\phi_r\right) \tag{4.1}$$

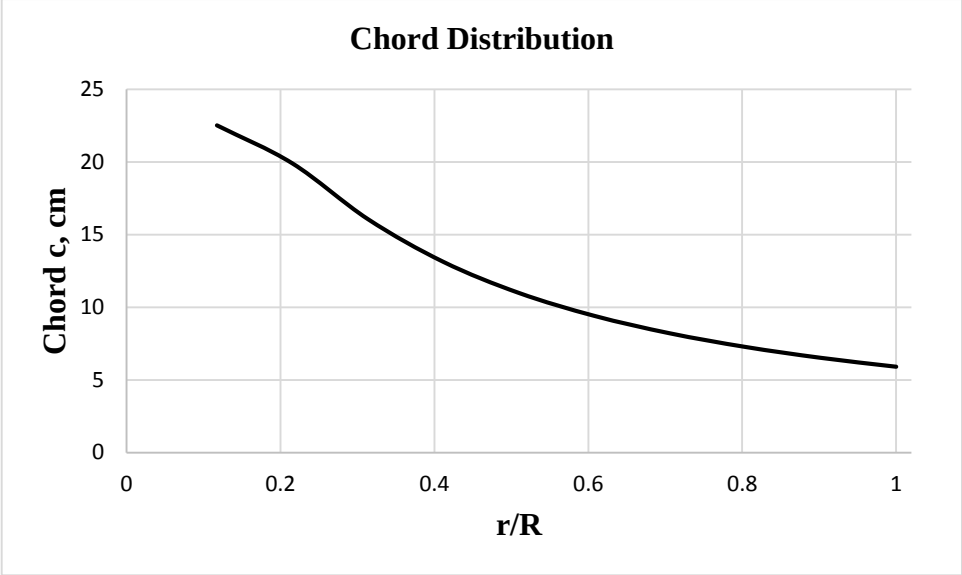

Fig 4.3 Chord distribution of the blade

Step 6: Discretize the blade into n elements **n=10**

Step 7: Choose an angle of attack α in such a way that its value is constant throughout the blade: **α=6°**

Step 8: Examine the lift C_L & drag coefficient C_D curves for the airfoil by considering Reynolds Number of 100,000.

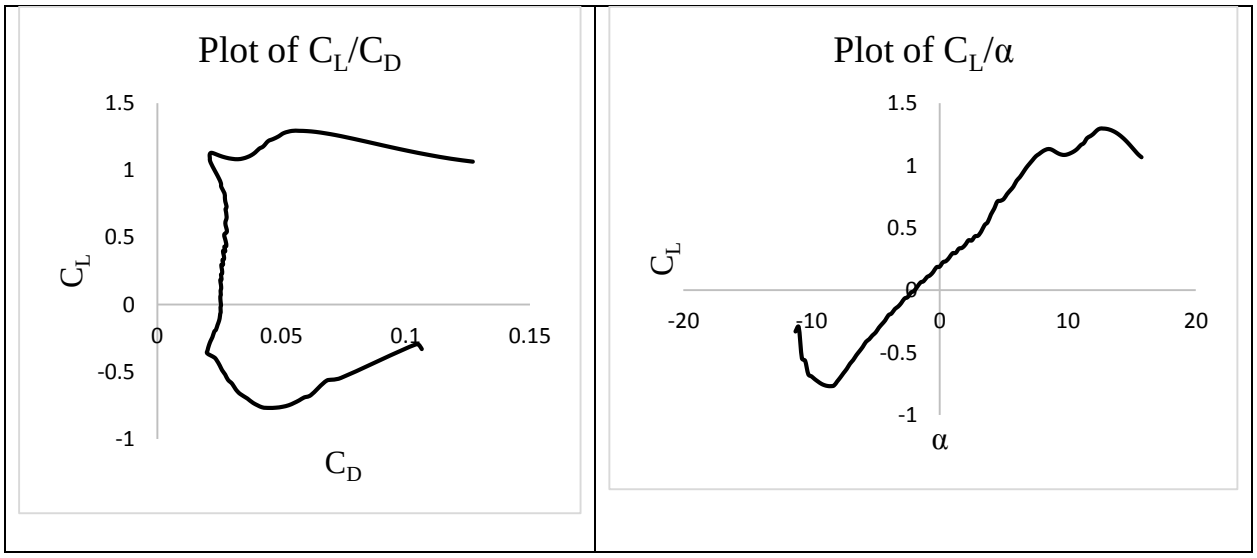

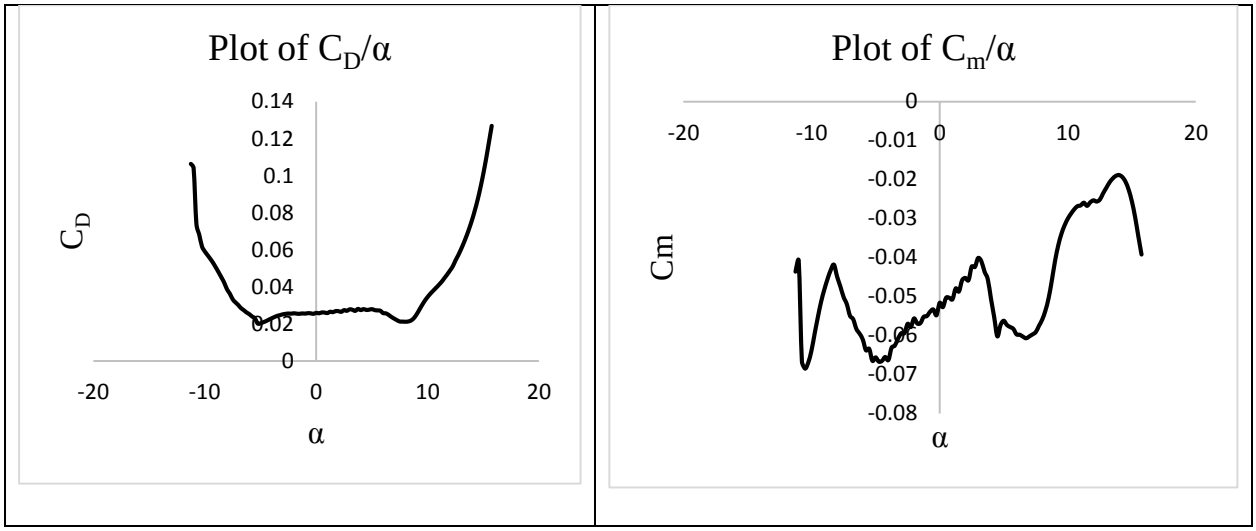

Fig 4.4 Plots of Lift, Drag and Moment Coefficients of NACA 63415

Step 9: Obtain the lift, drag, moment coefficients for the specified angle of attack of the blade:

C_m=-0.0597

C_L=0.8765

C_D=0.0258

Step 10: Obtain the angle of relative wind φ_r.

$$\phi = \frac{2}{3}\tan^{-1}\left(\frac{1}{\lambda_e}\right) \tag{4.2}$$

Step 11: Calculate the angle of blade twist θ_T, from the angle of attack and angle of relative wind. $\theta = \phi - \alpha$ (4.3)

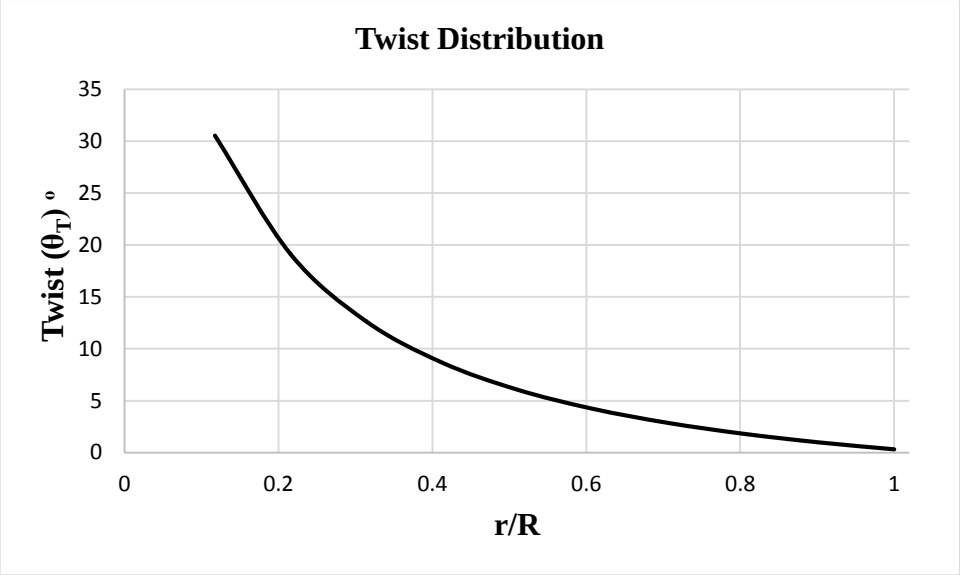

Fig 4.5 Twist distribution of the blade

4.2 Input Parameters

The parameters of the wind turbine blade considered in the present analysis are depicted in Table 4.1. The geometrical properties of the blade elements are tabulated in Tables A1 in the Appendix II and Inertial properties can be tabulated as shown in Table 4.2.

Table 4.1 Properties of the blade [24]

Material	**Glass Fiber Reinforced Plastic**
Mass density of the blade	1400 kg/m^3
Elastic Modulus of the blade	6 GPa
Poisson's Ratio	0.18
No. of Elements	10
No. of Elements at the root section	1
No. of Elements in the working region	9
Length of the blade	1.02m
Radius of the hub	0.06m

Table 4.2 Inertial Properties of the Blade at tip-speed ratio λ=6

Element	dr	A, cm^2	Twist θ	Ixx, cm^4	Iyy, cm^4	Izz, cm^4	Iyz, cm^4
1	0.12	8.365	0	11.137	5.568	5.568	0
2	0.1	42.394	29.825	934.172	196.041	738.131	339.058
3	0.1	30.701	15.891	504.374	53.747	450.626	130.524
4	0.1	20.193	10.671	217.006	13.286	203.719	38.015
5	0.1	13.745	7.379	99.700	4.206	95.493	11.849
6	0.1	9.815	5.145	50.477	1.944	48.533	5.248
7	0.1	7.311	3.539	27.863	1.071	26.792	2.661
8	0.1	5.637	2.332	16.501	0.457	16.044	0.519
9	0.1	4.470	1.393	10.349	0.278	10.071	0.159
10	0.1	3.627	0.643	6.800	0.181	6.619	0.0178

4.3 1-D Beam Finite Element Analysis Outputs

The blade under consideration has a variable cross section and 10 elements are taken, one near the root and nine along the blade working zone. By arresting the first node, 66 × 66 matrices reduce to 60 ×60 matrices. The computational work is carried out using MATLAB to find out the Global Mass and Global Stiffness matrices, giving boundary conditions, and Eigen value analysis is conducted. The following pseudo code highlights the main parts of the program.

Pseudo Code:

```
%Initialize the parameters
        Ae, le, E, ρ, Iy,  Iz,  Iyz,  J, G, ν
%Generate Global Stiffness and Global Mass Matrices
Loop:
        for     i=1:length(A)
                Compute [K]e, [M]e;
                r= (i-1)*6+1;
                GKs(r:r+11,r:r+11)=K;
                GK=GK+GKs;
                GMs(r:r+11,r:r+11)=M;
                GM=GM+GMs;
        end
%Do modal reduction by imposing boundary conditions
Loop:
        for     i=7:66
                for     j=7:66
                        Kr (i-6,j-6)=GK (i,j);
                        Mr (i-6,j-6)=GM (i,j);
                end
        end
%Find out Eigen Values and Eigen Vectors
        A1=Kr/Mr;
        [y,d2]=eig(A1);
        Loop:
        for     i=1:60
                D1(i)=d2(I,i);
        end
        [EV,index]=sort (D1);
%Print the 1st Five Natural Frequencies
        NF=sqrt(EV)/(2*pi);
        fprintf('First five Natural Frequncies /n');
        fprintf('%f\n%f\n%f\n%f\n%f', NF(1), NF(2), NF(3), NF(4), NF(5));
```

The MATLAB program is implemented on a Windows 8.1 operating system with 4 GB RAM and Intel i5 2.6GHz processor. The results obtained by the eigen value analysis are tabulated in Table 4.4.

4.3 Modal Characteristics of the blade from ANSYS 15.0

Using ANSYS 15.0 workbench, the modal analysis tool is invoked, the material properties are given, and the geometry is imported into the workbench. Fig 4.3 shows the mesh details for 3-

D model using Tetrahedral beam elements. The total deformation and first five natural frequencies are obtained and their mode shapes are recorded.

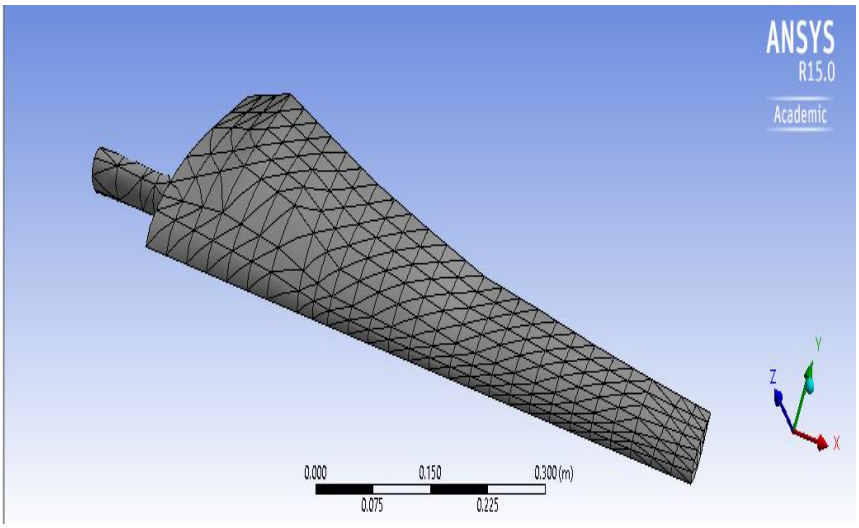

Fig 4.6 Mapped Mesh of the blade

Modal analysis is conducted and the first five natural frequencies are shown in Table 4.2 in comparison with 1-D model. The results are found to be in close comparison by both methods.

Table 4.4 Modal Characteristics of the Blade

Mode	**1-D Beam Element, Hz**	**3D Solid Model, Hz**
1	11.63185	11.344
2	15.39532	15.335
3	31.5512	31.202
4	77.95628	75.913
5	124.99	124.79

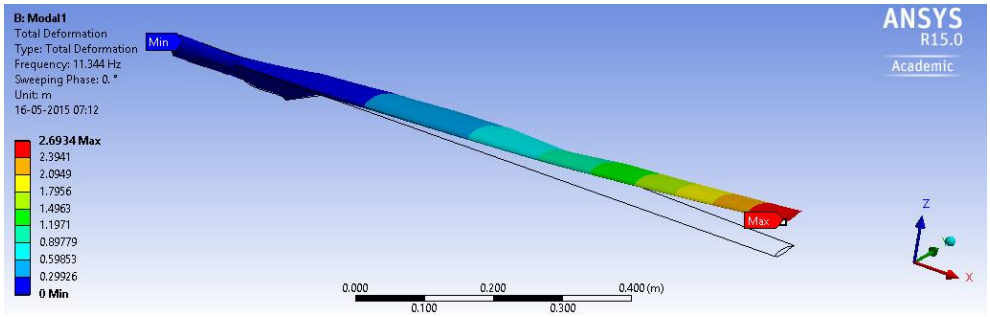

Fig. 4.7a 1st Flapwise Bending Mode shape

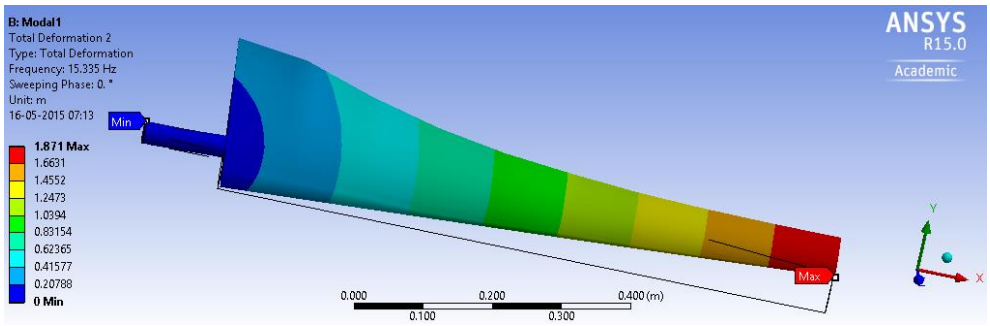

Fig 4.7b 1st Edgewise Bending Mode shape

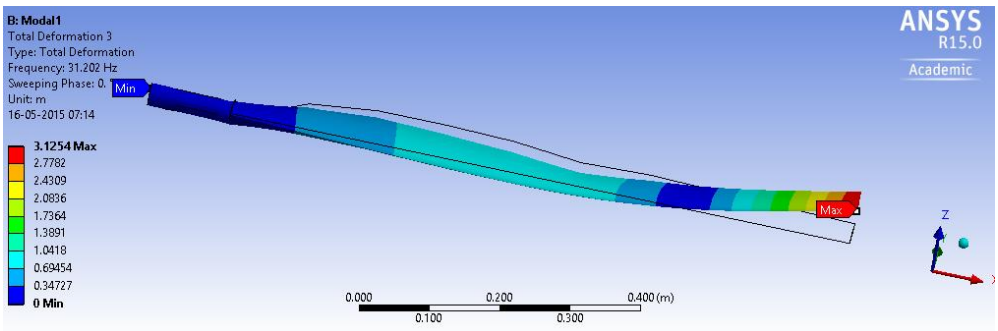

Fig 4.7c Combined Bending Mode shape

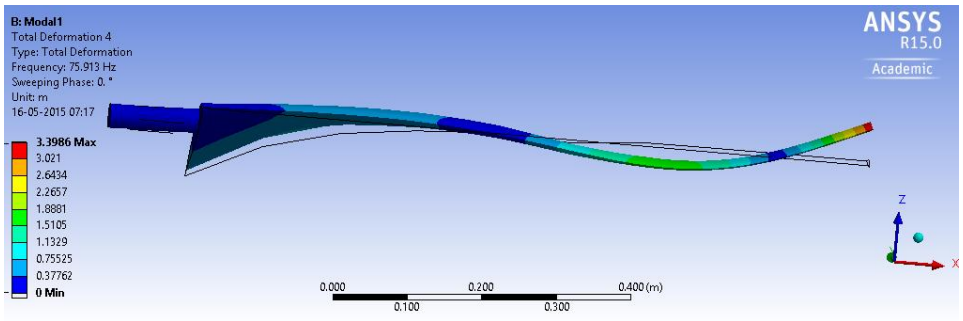

Fig 4.7d 2nd Flapwise Mode shape

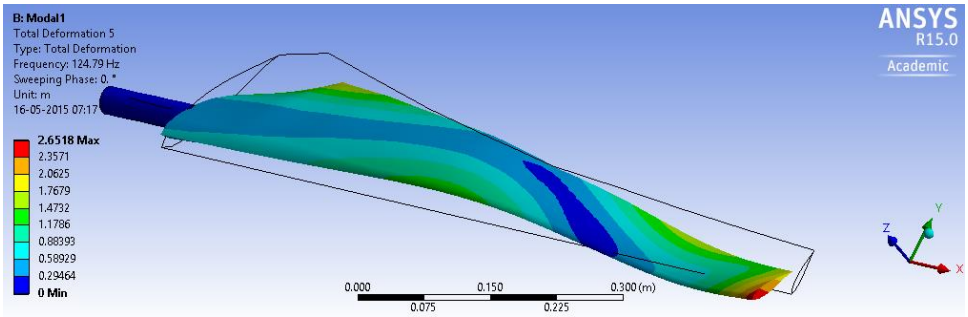

Fig 4.7e Torsional Mode shape

Fig 4.7 Mode shapes observed in Modal analysis conducted by ANSYS

Aerodynamic and elastic forces occurring cause aero-elastic vibrations, and these vibrations arise around all three axes. First, the rotor blades generally vibrates across the plane in which rotor rotates in flap-wise direction (1st mode, Fig 4.7a). Further, rotor blades vibrate in the plane edge wise (1st mode, Fig 4.7b). Further in mode shapes Fig 4.7c and Fig 4.7d, the blades simultaneously vibrate along 2 directions (sway). The mode shape in Fig 4.7e shows additional torsional vibration along the x axis.

4.4 Effect of Rotational Speed on Natural Frequencies

Constant speed Analysis is helpful to examine the effect of system parameters on the natural frequencies of undamped free vibrations of a tapered wind turbine blade rotating at various speeds from 0rpm to 50 rpm.

Graphs are plotted as shown in Figures 4.8 to 4.10 between the frequency of flap-wise bending, Edge-wise bending and torsional bending modes with increase in the rotational speed of the blade.

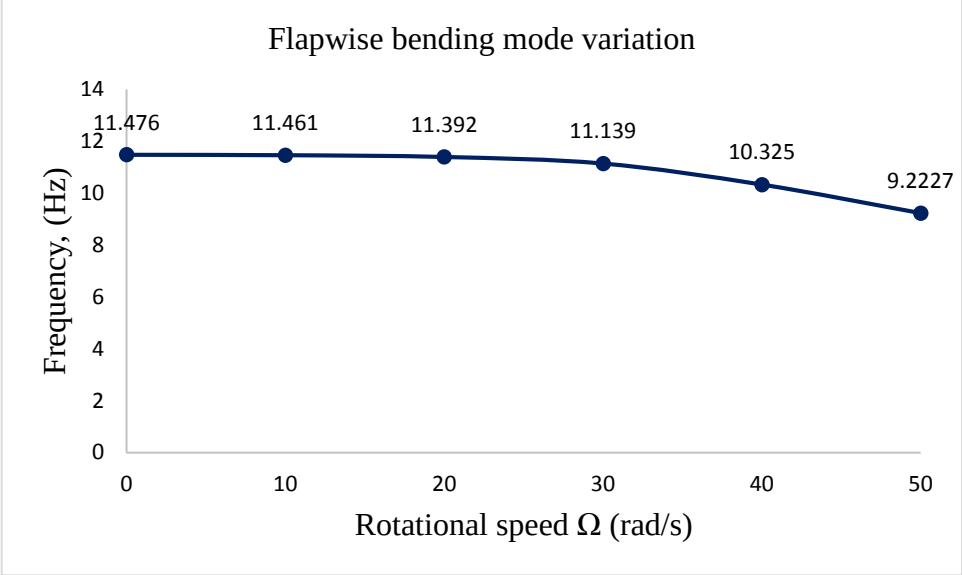

Fig 4.8 Variation of Flap wise bending mode with respect to rotational speed

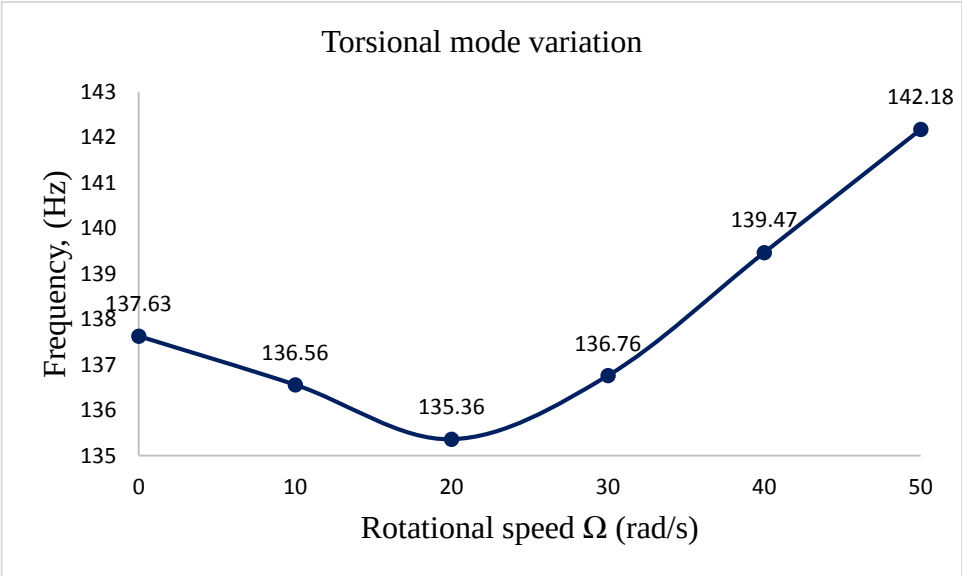

Fig 4.9 Variation of Torsional bending mode with respect to rotational speed

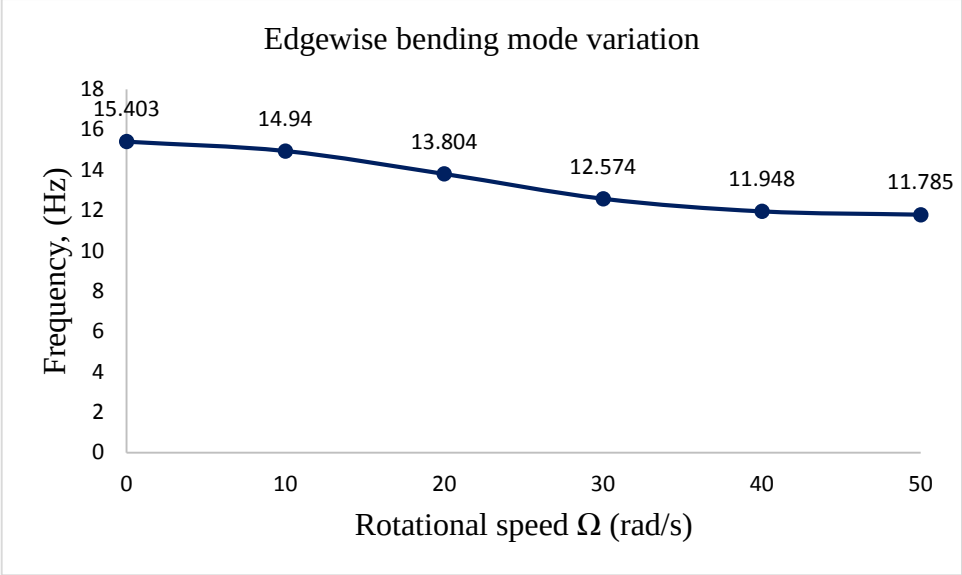

Fig 4.10 Variation of edgewise bending mode with respect to rotational speed

It is observed from the figures 4.8 to 4.10 the value of natural frequencies are more in torsional bending mode compared to the flap-wise bending mode and edge-wise bending mode. It is also seen that in the torsional mode, the trend of natural frequencies are seen to decrease until 20 rpm and then increase. This can be noted that optimal speed of the wind turbine operation must be more than 20 rpm in order to ensure safety of the component.

4.5 Effect of tip speed ratio on the chord & Twist distributions of the blade

Graphs are plotted between the distances from the root to the chord length as shown (Figure 4.11) and twist distributions (Figure 4.12) for different values of tip speed ratios.

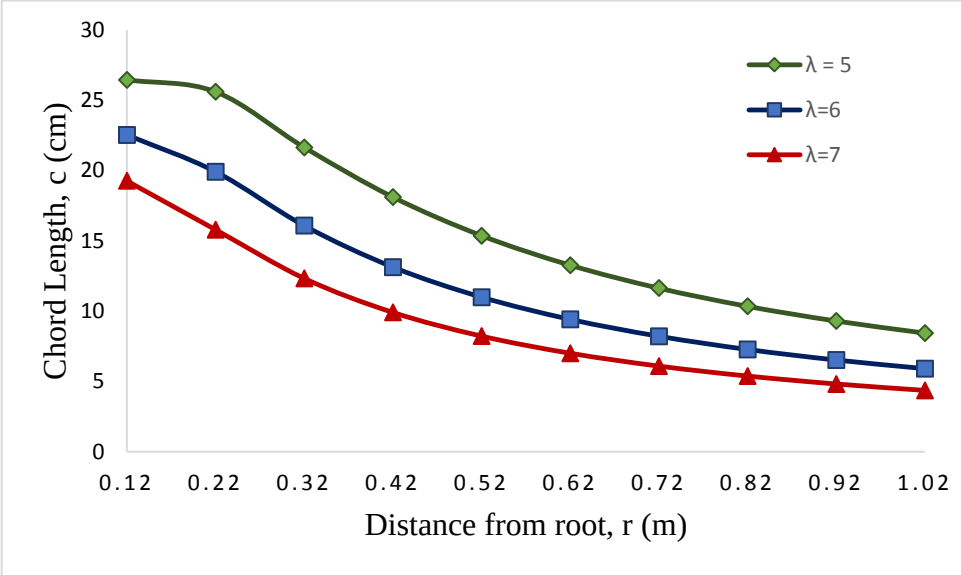

Fig 4.11 Chord distribution variation for different taper ratios.

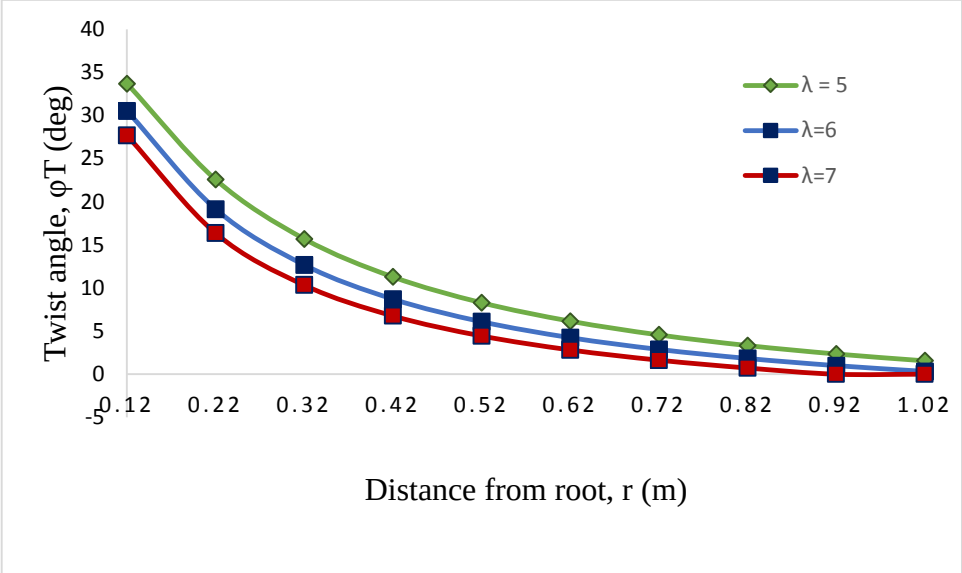

Fig 4.12 Twist distribution variation for different taper ratios

From the figure 4.11 it is observed that whenever the tip speed ratio (λ) increases the chord length also increases. From the figure 4.12 it is observed that whenever the tip speed ratio (λ) is increases the twisting angle is decreasing. This corresponds to the fact that larger tip speed ratio blades must have lesser chord length to ensure that they rotate faster reducing the overall centrifugal forces of the blade.

4.6 Effect of tip speed ratio on the modal characteristics of the blade

Graph is plotted between the first five natural frequencies and mode shapes for different tip speed ratios of 5,6 and 7 from the results of modal analysis.

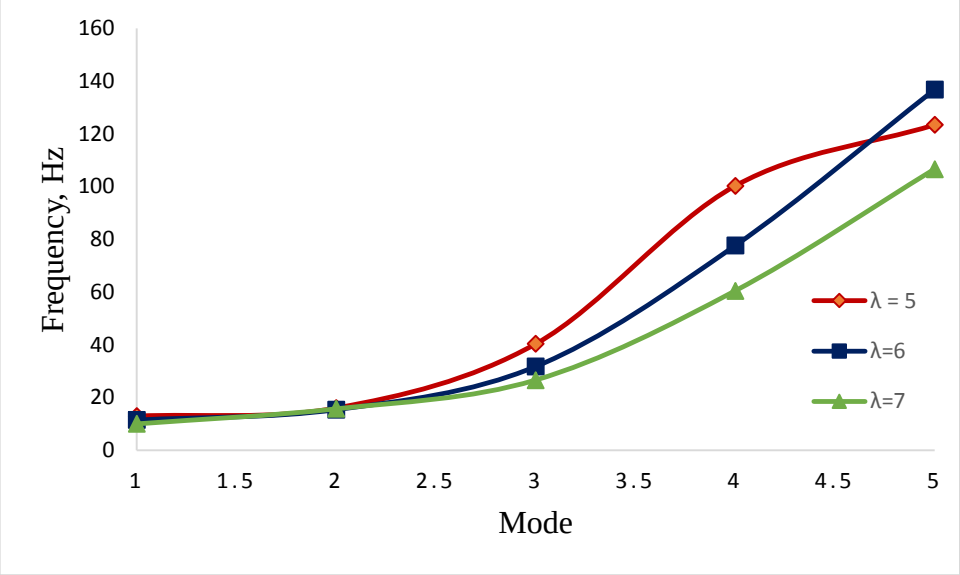

Fig 4.13 Modal Variation for different taper ratios

From the figure 4.13 it is observed that lower tip speed ratios have higher values of modal frequencies. Compared to λ=6 & 7, where the trend of modal frequencies are gradually increasing, the frequencies are found to be increasing at gradual mode until 4th natural frequency for λ=5 and then slope of the curve is observed to decrease.

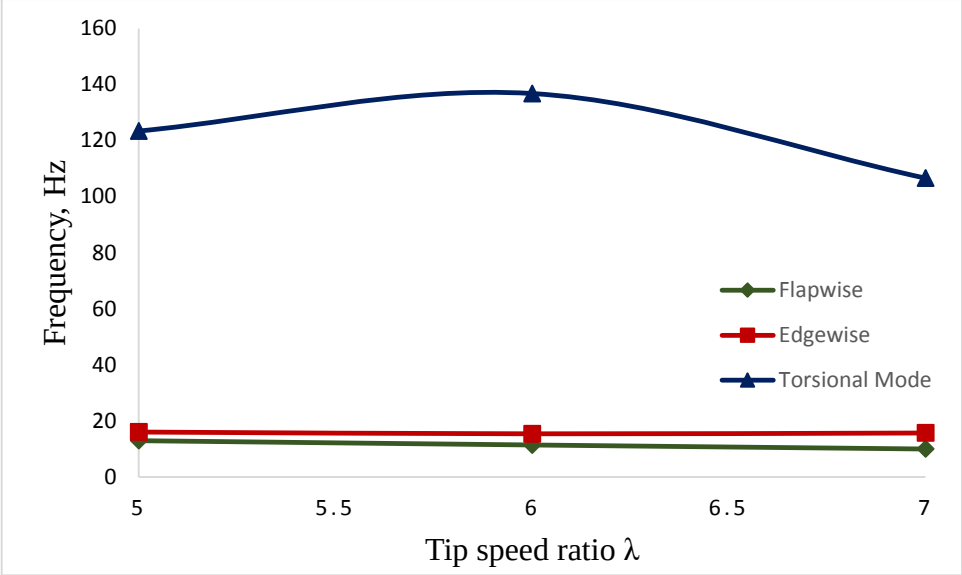

Fig 4.14 Variation of flap wise, edgewise and torsional modes for different taper ratios.

For the plot drawn (Figure 4.14) to observe the pattern of flap-wise, edge-wise and Torsional modes at different taper ratios, it is seen that the natural frequency values for the torsional mode the frequency are high and the curve reaches a peak of 136Hz at $\lambda=6$ and then decreases. The effect of edge-wise modes with increase of taper ratio is found to be negligible and the flap-wise modes are found to gradually decrease from 13Hz to 9Hz.

4.7 Dynamic response Analysis

Dynamic response of the blade subjected to aerodynamic, centrifugal, gravity and gyroscopic loads is computed by using Newmark time integration algorithm (parameters $\alpha=0.25$ & $\delta=0.5$). The MATLAB code employed is provided in the Appendix IV.

The FFT spectrum of the blade dynamic response of the displacement in x direction at the blade tip is shown in Fig 4.15.

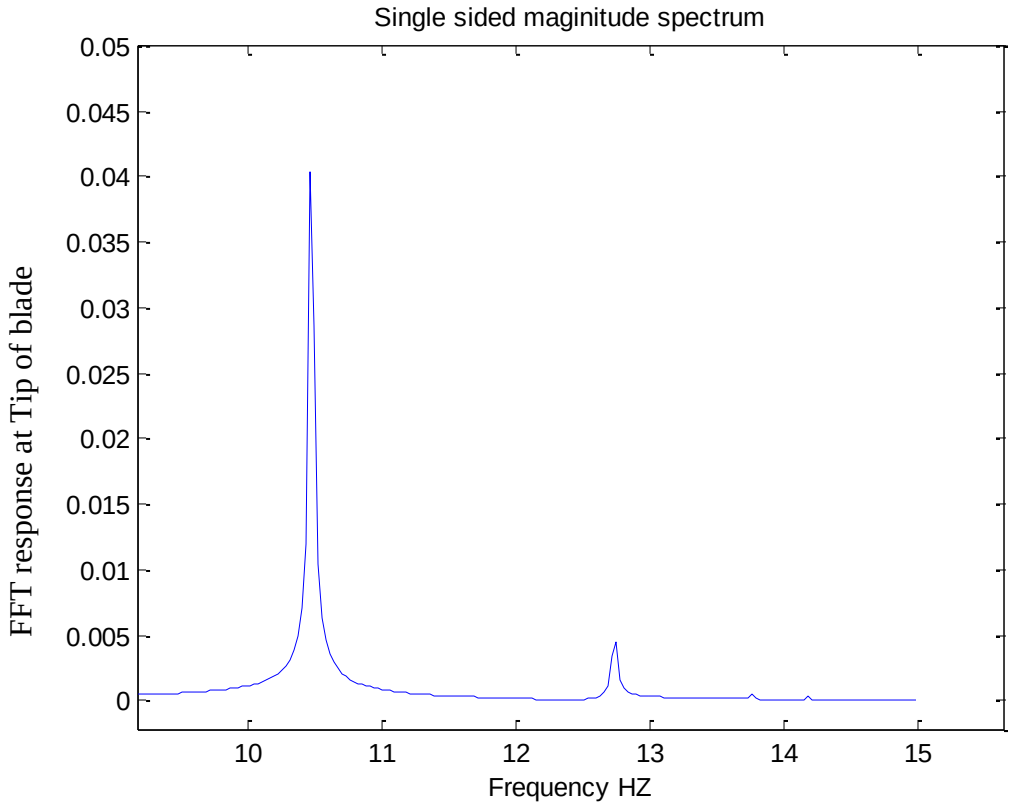

Fig 4.15 FFT spectrum of blade dynamic response.

It shows that the fundamental frequency f_1=10.46 Hz and second frequency f2=12.7 Hz for rotational speed (Ω) of 50 rad/s. These frequencies are found to be slightly more than the free vibration frequency due to the additional centrifugal stiffening & geometric stiffening effect due to the rotational velocity of the blade.

The Edge-wise flexure angle response (β) and the flap-wise Flexure Angle response (γ) are shown in the Figure 4.16 and Figure 4.17.

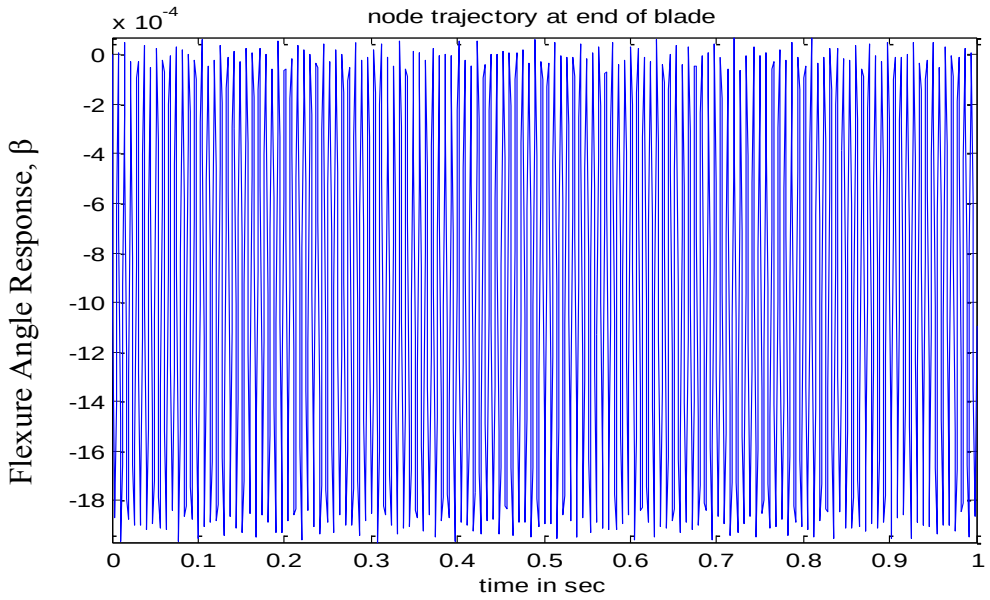

Fig 4.16 Edge-wise beating at blade end

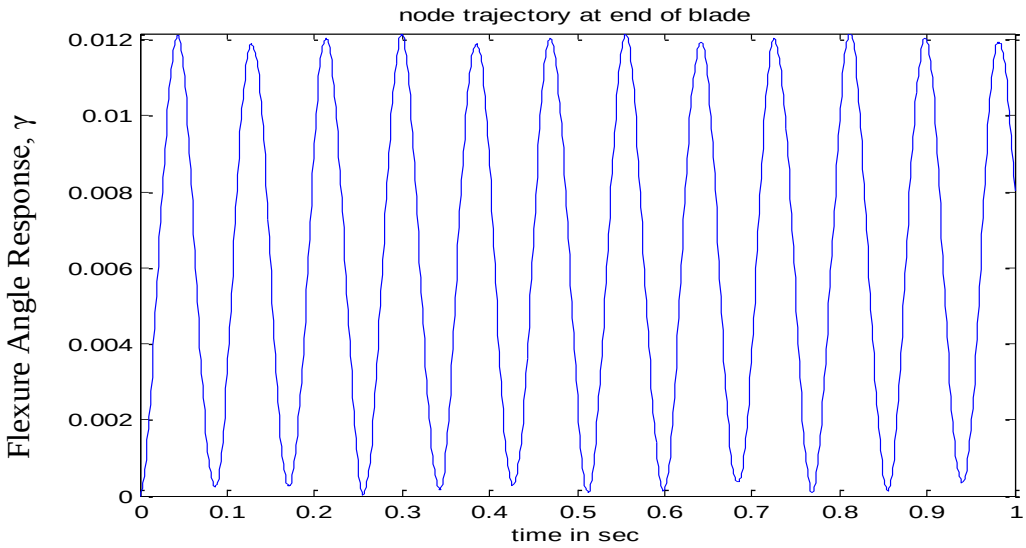

Fig 4.17 Flap-wise beating at the blade end

It is observed that amplitudes of edge-wise beating is less (in range of $1*10^{-4}$) but the frequency of vibration is more whereas in the flap-wise beating, the amplitudes are more (in order of 0.012) but frequency of vibration is less.

The edge-wise and flap-wise beating of the blade subjected to only aerodynamic loads are shown in the Fig 4.18 gives the edgewise beating and Fig 4.19.

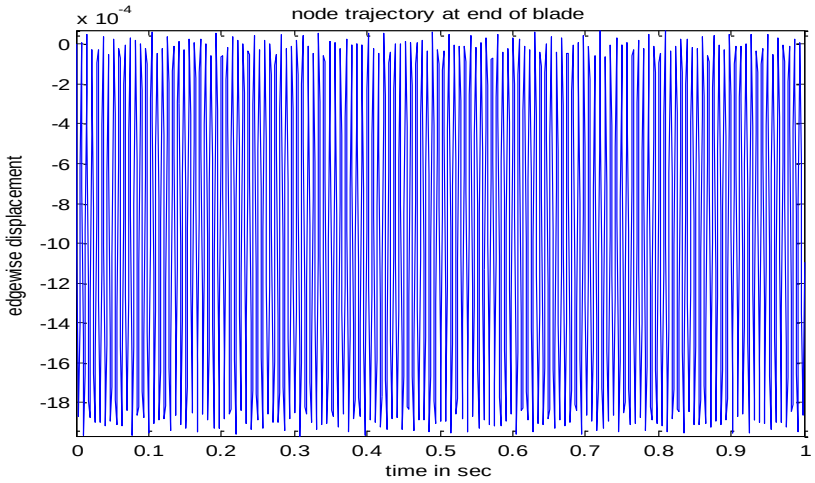

Fig 4.18 Edge-wise beating at blade end subjected to only aerodynamic loads

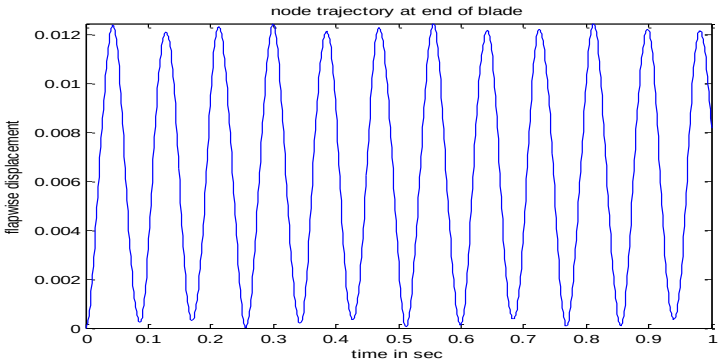

Fig 4.19 Flap-wise Beating at the blade end subjected to only aerodynamic loads

It is observed that from comparison of Figures 4.16,4.18 and 4.17, 4.19 that aerodynamic loads contribute most of the loading on the blade. There is negligible difference with responses of considering all loads, and aerodynamic loads alone. But since aerodynamic load are profile dependent, and not time dependent, its effect on dynamic displacement response is null.

Figures 4.20 shows dynamic response of blade in x direction & Figure 4.21 shows the edge-wise beating response of blade subjected to only centrifugal loads.

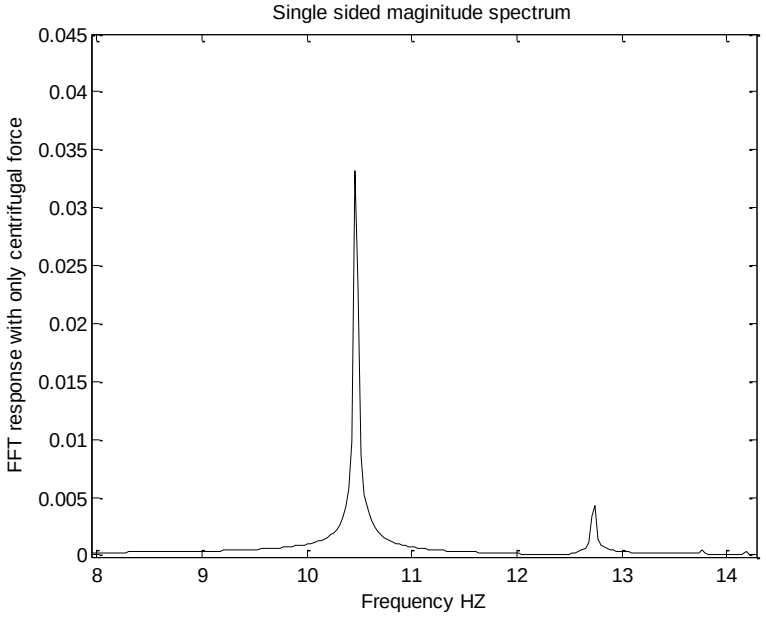

Fig 4.20 FFT spectrum of blade dynamic response subjected to only centrifugal loads.

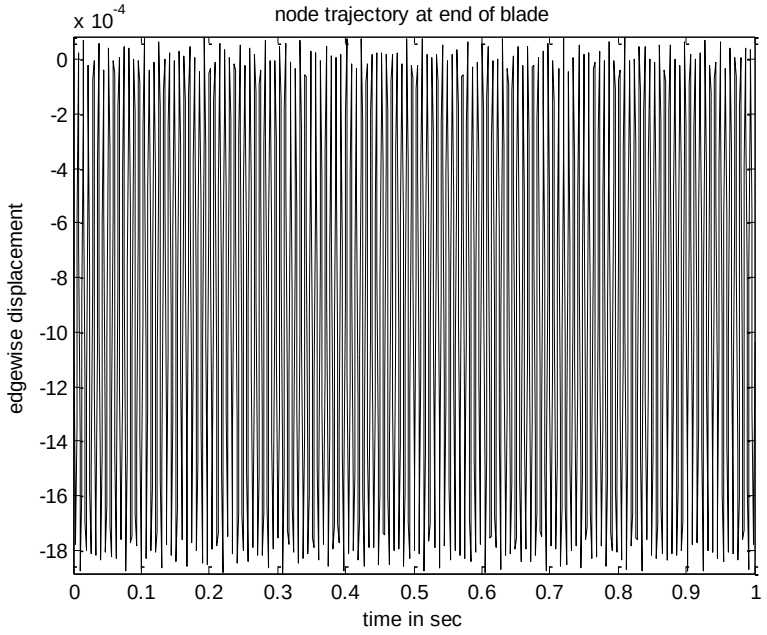

Fig 4.21 Edge-wise beating at blade end subjected to only centrifugal loads

The dynamic response shows a fundamental frequency of 10.43 Hz and second fundamental frequency of 12.8 Hz. The amplitude of the vibration is lesser compared to the blade dynamic response when subjected to all loads (Fig 4.15) The flap-wise response is found to be zero when subjected to only centrifugal forces while there is no significant difference between the edgewise beating.

Figure 4.22 shows the dynamic response of blade in x direction & Figure 4.23 shows the flap-wise beating response of blade subjected to only gravity loads.

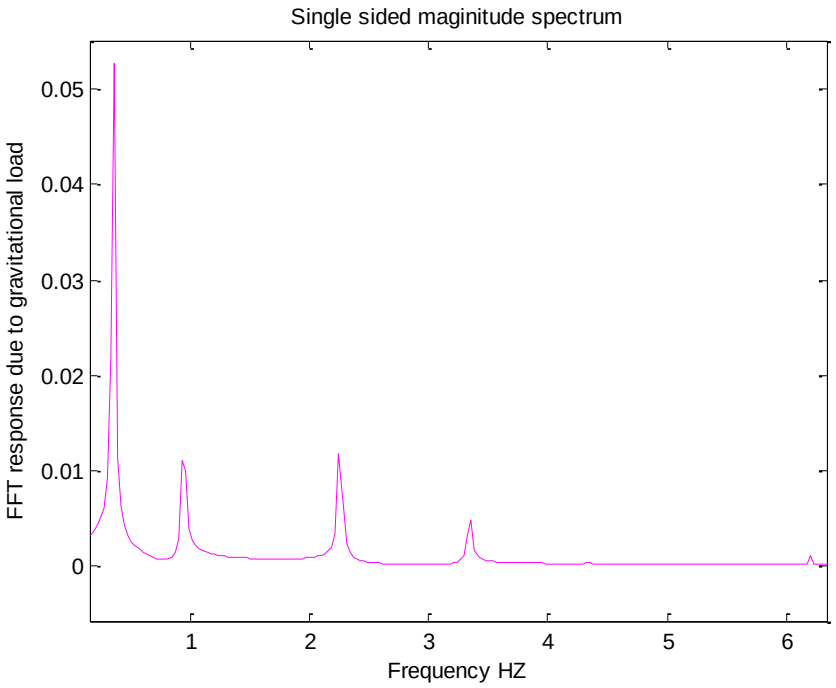

Fig 4.22 FFT spectrum of blade dynamic response subjected to only centrifugal loads.

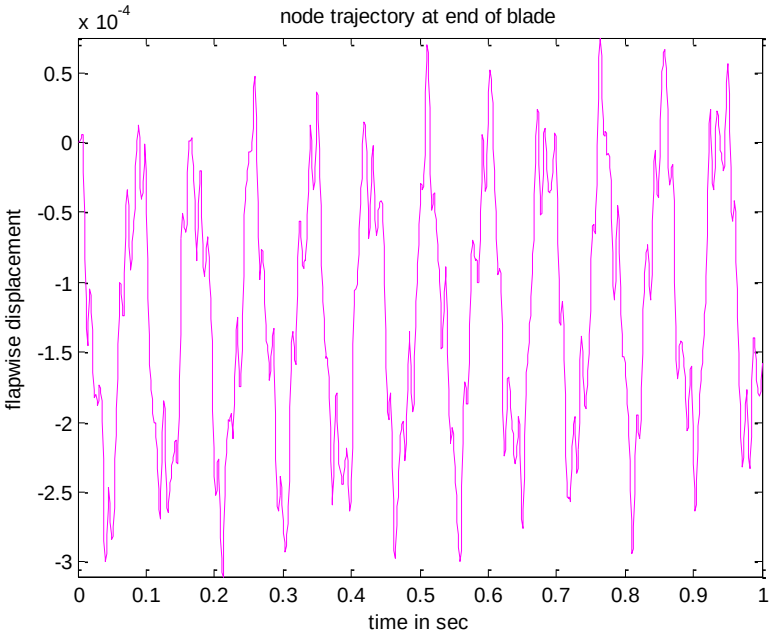

Fig 4.23 Flap-wise beating at blade end subjected to only centrifugal loads

From the Figure 4.22 it can be observed that a range of frequencies with small amplitudes occur within short frequency range. The Flap-wise beating (Figure 4.23) is irregular in nature. Since acceleration due to gravity acts in the vertical y direction, the edgewise beating doesn't occur when the blade is subjected to only gravity loads.

Chapter-5

Conclusion

5.1 Summary

High speed rotating wind turbine blade dynamic analysis has been conducted in this work. From the available literature, various forces acting on the blade are accounted and the tapered-twisted aerofoil profile of the blade was generated as a 3D model. By computing element wise cross sectional details from 3D model, a one dimensional finite element beam modelling was considered to discretize the blade from the hub center. Also, a method proposed in literature for the blade dimensions selection was adopted to get the optimum chord and twist angle when the blade tip speed ratio, airfoil type & length of the blade are specified as inputs. The entire work concentrates on the beam finite element modelling of the blade. The modal and transient analysis studies are conducted using 10 beam elements with 6 degrees of freedom per node. It was considered that the blade is fixed at the hub rigidly with five degrees of freedom constrained. The effect of rotational speed on variations of the natural frequencies with the system parameters are given and it is found that with increase in speed, torsional modes vary at larger extent compared to flap-wise and edge-wise modes. Three blade models having tip speed ratios of λ=5, 6 and 7 are considered and the effect of tip speed ratio on the chord & twist distributions and on the modal characteristics are studied. The results show that at tip-speed ratio (λ=6), the torsional frequencies are more. Dynamic response by considering various loading conditions of blade displacement, and edge-wise, flap-wise beating responses are obtained and studied. Results are very interesting

indicating the effects of aerodynamic load, centrifugal loads and gravity on the tip response. These results are helpful for the design of blades to avoid resonant conditions.

5.2 Future Scope

As a future scope, approximate solution methods for the continuous system of equations have to be applied, so as to validate the result of finite element modelling. Material issues should be introduced to know their effects on dynamic characteristics and failure prediction approaches using polymer composite materials. Testing and analysis of blades can be done on varying climatic conditions such as high humidity, cold regions or high temperature zones. The fatigue, buckling analysis and localized surface roughness on the current blade models determining the structural integrity in real-time approaches, the tower's structural and dynamic interactions must also be taken into account. Fluid structure interaction studies can be done for the flow of wind around the blades and possibilities of formation of eddies and rotor wakes. The area of improving the material characteristics by using layered composites itself is a huge research field for the interested because it offers innumerable combinations of materials to be used to improve effectiveness of the blade.

References

1. Nitin Tenguria, N.D. Mittal, Siraj Ahmed, "*Aerodynamic Design of a HAWT Blade for Indian Wind Condition",* International Journal of Advances in Engineering, Science & Technology (IJAEST), Vol. 1 No.7, September – November 2011, pp 37-41.
2. John McCosker, *"Design and optimization of a small wind turbine",* Rensselaer Polytechnic Institute, Hartford, Connecticut, December 2012, pp 1-56.
3. M. Anjali, C. Tara Sasanka, Ch. Deva Raj, K. Ravindra, "*Meta Heuristic Method for the Design Optimization of a Wind Turbine Blade",* International Journal of Current Engineering and Technology, ISSN 2277 – 4106, Special Issue -3, April 2014, pp 175-179.
4. Chalothorn Thumthae, Tawit Chitsomboon, "*Optimal Pitch for untwisted blade horizontal axis wind turbine",* 2nd Joint International Conference on "Sustainable energy and environment SEE, November 2006, pp 1-6.
5. Juan Mendez, David Greiner, "*Wind blade chord and twist angle optimization by using genetic algorithms",* Intelligent systems & Numerical Applications in Engineering, Spain 2011, pp 4-19.
6. Wang Yongzhi, Li Feng, Zhang Xu, Zhang Weimin, "*Composite Wind Turbine Blade aerodynamic and structural integrated design optimization based on RBF meta-model",* China Academy of Aerospace Aerodynamics, May 2007, 830: 10-18.
7. K. Dykes, A. Platt, Y. Guo, et al. *"Effect of Tip speed constraints on the optimized design of a wind turbine",* National renewable energy laboratory, NREL/TP-5000-61726, October 2014, pp 1-77.
8. Grant Ingram, "*Wind Turbine Blade Analysis using the Blade Element Momentum Method, Version 1.1",* October 18, 2011, pp 1-21.

9. Naishadh G. Vasjailiya, Sathya N. Gangadharan, "*Aero-structural design optimization of composite Wind Turbine Blade",* 10th World Congress, 2013, pp 201-217.
10. Ahmad Sedaghat, M. El Haj Assad, Mohamed Gaith, "*Aerodynamics Performance of continuously variable speed horizontal axis wind turbine with optimal blades",* Energy Vol 77, December 2014 752-769.
11. Scott Larwood, C.P. Van Dam, Daniel Schow, "*Design Studies of swept wind turbine blades",* Renewable Energy 71 (2014) 563 – 571.
12. K. Turgut Gursel, Tufan Coban, Aydogan Ozdamar, "*Vibration Analysis of rotor blades of a farm wind power plant",* Mathematical and Computational applications, Vol. 17, No. 2, 2012, pp. 164-175.
13. Gunner C. Larsen, Morten H. Hansen, Andreas Baumgart, Ingemar Carlen, "*Modal Analysis of Wind Turbine Blades",* Risφ National Laboratory, Roskilde, Denmark February 2002, pp 1-72.
14. Chao Liu, Dongxiang Jiang and Jie Chen, "*Vibration Characteristics on a Wind Turbine Rotor using Modal and Harmonic Analysis of FEM",* 978-1-4244-8921-3/10 IEEE 2010, pp 1-5.
15. O Pabut, G Allikas, H Herranen, R Talalaev, K Vene, "*Model Validation and structural analysis of a small wind turbine blade",* 8th International DAAAM Baltic Conference, Industrial Engineering, 19-21 April 2012, pp 1-10.
16. Saad Sami, Behzad Ahmed Zai, M. Amir Khan,"*Dynamic Analysis of a 5KW Wind Turbine Blade with experimental Validation",* Journal of Space Technology, Vol. 4, No-1, July 2014, pp 82-87.
17. Fangfang Song, Yihua Ni, Zhiqiag Tan, "*Optimization Design, Modelling and Dynamic Analysis for Composite Wind Turbine Blade",* International Workshop of Automobile, Power and Energy Engineering, Procedia Engineering, 16 (2011) 369-375.

18. Zhu Jie, Cai Xin, Pan Pan, "*Static and Dynamic Characteristics Study of Wind Turbine blades",* Advanced Materials Research Vols 433-440 (2012) pp 438-443.
19. Xin Cai, Pan Pan, Jie Zhu, Rongrong Gu, "*The Analysis of the aerodynamic character and structural response of Large Scale Wind Turbine Blades",* 6, , Journal of Energy, 2013, pp 3134-3148.
20. T. Inoue, Y. Ishida and T. Kiyohara, "*Non Linear Vibraiton Analysis of wind turbine blade (occurrence of the super harmonic resonance in out of plane vibrations of the elastic blade",* J. Vibration and acoustics, Trans. ASME, Vol. 134, pp. 0310091 -10, 2012.
21. L. Li, Y. Li, Q. Liu and H. Lv, "*Dynamic Characteristics of lag vibration of wind turbine blade*", Acta Mechanica Solids Sinica, Vol. 26, pp. 592 – 602.
22. L. Li, Y. H. Li, Q. K. Liu, H. W. Lv, "*A Mathematical Model for Horizontal axis wind turbine blades",* Applied mathematical Modelling 38 (2014) 2695-2715.
23. L. Li, Y. H. Li, H. W. Lv, Q. K. Liu, "*Flapwise dynamic response of a wind turbine blade in super-harmonic response",* Journal of Sound and Vibration 331 (2012) 4025-4044.
24. Hamdi H, Mrad C, Hamdi A, Nasri R, "*Dynamic response of a horizontal axis wind turbine blade under aerodynamic, gravity and gyroscopic effects",* Applied Acoustics, July 2013, pp 1-11.
25. V. Karadag, "*Dynamic analysis of Practical Blades with Shear center effect",* Journal of Sound and Vibration (1984) 92(4), 471-490.
26. Martin Nymann Svendsen, Steen Krenk, jan Hogsberg, "*Resonant Vibration control of rotating beams",* Journal of Sound and Vibration 330 (2011) 1877-1890.

27. M. Keerthana, M. Sriramkrishnan, T. Velayutham, A. Abraham, S. Selvi Rajan, K. M. Parammasivam, "*Aerodynamic analysis of small Horizontal axis wind turbine using CFD",* Journal of Wind and Engineering, Vol. 9, No.2, July 2012, pp. 14-28.
28. Yangfeng Wang, Ming Liang, Jiawei Xiang, "*Damage detection method for wind turbine blades based on dynamic analysis and mode shape difference curvature information",* Mechanical Systems and signal processing 48 (2014) 351-367.
29. Mu Chu, Philip Clausen, "*The Dynamic Response of Small Horizontal Axis Wind Turbine Blade operating in Highly Turbulent Flow",* Solar 2014, 52nd Annual conference of the Australian Solar Council, Melbourne, May 2014, 2323 1-17.
30. Yuqiao Zheng, Rongzhen Zhao, Hong Liu, "Dynamic response of flexible wind turbine blade", Telkomnika, Vol 11, No. 12, December 2013, pp, 7052-7057.

Appendix I

NACA Airfoil Designations

I.1 NACA 4 digit series

The NACA 4 digit series is generally denoted by **$NACA_{mpxx}$,**

Where,

- m indicates max. value of mean line coordinates in % of chord,
- p is the leading edge distance to location of maximum camber in tens of chord
- xx indicates the thickness of the section as % of chord.

From getting the above parameters, the camber line can be expressed as

$$\frac{Z_c}{c} = \frac{m}{p^2}\left(2p\xi - \xi^2\right) \qquad \text{for } 0 \le \xi \le p \qquad \text{(A.1)}$$

$$\frac{Z_c}{c} = \frac{m}{(1-p)^2}\left(1 - 2p + 2p\xi - \xi^2\right) \qquad \text{for } p \le \xi \le 1 \qquad \text{(A.2)}$$

The Thickness distribution is given by,

$$Z_{th} = 5c(0.2969\ \xi^{0.5} - 0.1260\ \xi - 0.3516\ \xi^2 + 0.2843\ \xi^3 - 0.1015\ \xi^4) \qquad \text{(A.3)}$$

The coordinates of the airfoil profile can be obtained as:

$$X_u = X - Z_{th}\sin\theta_a$$
$$Z_u = Z + Z_{th}\cos\theta_a \qquad \text{(A.4)}$$

$$X_l = X + Z_{th}\sin\theta_a$$
$$Z_l = Z - Z_{th}\cos\theta_a \qquad \text{(A.5)}$$

Where (X_u, Z_u) are the coordinates of upper surface of airfoil, and (X_l, Z_l) are the coordinates of lower surface of airfoil

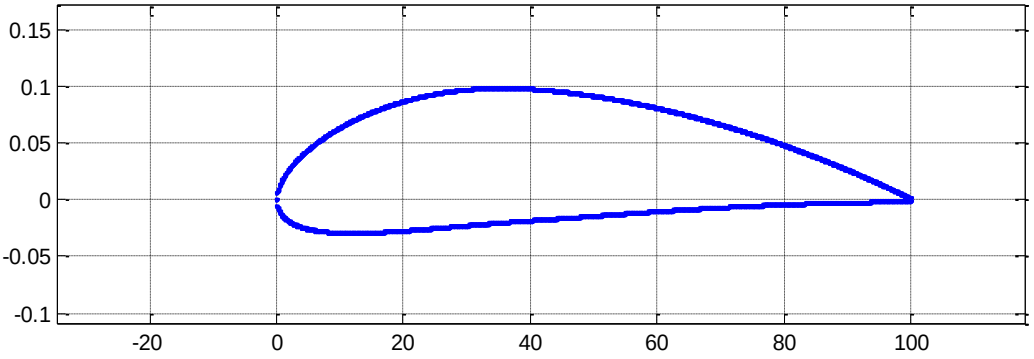

Fig A1 Aerodynamic profile of NACA 4412 profile

I.2 NACA 63nnn series:

NACA 63nnn series are slowly gaining importance as profiles for wind turbineas they can operate for less speed turbines giving optimal generation of power.

For the NACA 63nnn series, the general notation is **NACA6p-lxx.**

Where,

- 6 indicates the series name,
- p is the distance of where pressure is minimum on chord in terms of tens of chord length,
- The digit l indicates the design lift coefficient in tenths of chord.
- The two digits xx indicate the thickness of section as % of chord.

The Basic camber line equations (when axial induction factor is 0, uniform load is given over the span of chord), are given by:

$$\frac{Y}{c} = \frac{C_L}{4\pi}\left[\left(1-\frac{X}{c}\right)\ln\left(1-\frac{X}{c}\right)+\frac{X}{c}\ln\left(\frac{X}{c}\right)\right] \tag{A.6}$$

$$\frac{dy}{dx} = \frac{C_{Li}}{4\pi}\left[\ln\left(1-\frac{x}{c}\right)-\ln\left(\frac{x}{c}\right)\right] \tag{A.7}$$

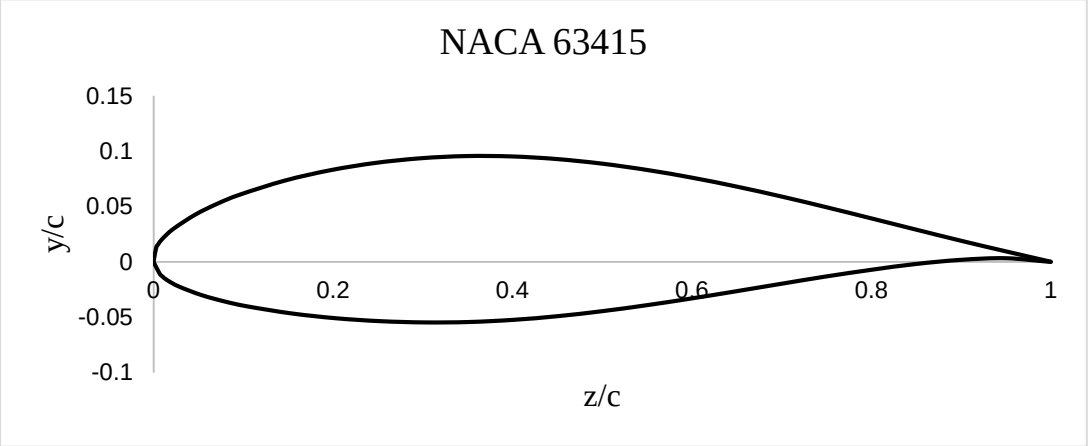

Fig A2 Profile of NACA 63-415 airfoil drawn in MATLAB

The NACA 63nnn series have gained prominence as profiles of modern composite wind turbine blades due their advantage of higher power coefficient. Thus these are replacing conventional profiles of blades suchas NACA 4digit and 23xxx series.

Table A1 Coordinate data of NACA 63415 Airfoil

Coordinates of NACA 63415 profile			
Upper Surface		**Lower Surface**	
X_u	**Z_u**	**X_l**	**Z_l**
0	0	0	0
0.00525	0.01585	0.00975	-0.0131
0.02198	0.02964	-0.0222	0.02802
0.0466	0.04264	0.0534	-0.03
0.09647	0.06077	0.10353	-0.0401
0.19705	0.08279	0.20295	-0.051
0.298	0.09362	0.302	-0.0547
0.39905	0.09527	0.40095	-0.0524
0.5	0.08871	0.5	-0.0446
0.6007	0.07595	0.5993	-0.0331
0.70106	0.05877	0.69894	-0.0199
0.80102	0.039	0.79989	-0.0072
0.90059	0.01884	0.89941	0.00184
1	0	1	0

Appendix II

Table A1 Geometrical Properties of Blade Elements obtained from initial program for Tip speed ratio λ=5.

r	λ_r	C_L	C_D	Cm	c_e	φ_r (deg)	α (deg)	θ_T	V	C_y	C_z	dF_t	dF_d	dM
0.12	0.588	0.8765	0.0258	-0.0597	0.264	39.68	6	33.68	5.7161	0.5796	0.6909	0.3066	0.36556	-0.0083
0.22	1.078	0.8765	0.0258	-0.0597	0.255	28.55	6	22.55	5.9060	0.4416	0.7821	0.2414	0.42757	-0.0083
0.32	1.568	0.8765	0.0258	-0.0597	0.216	21.67	6	15.67	6.9853	0.3477	0.8240	0.2248	0.53276	-0.0083
0.42	2.058	0.8765	0.0258	-0.0597	0.181	17.27	6	11.27	8.3485	0.2848	0.8446	0.2201	0.65265	-0.0083
0.52	2.549	0.8765	0.0258	-0.0597	0.153	14.28	6	8.280	9.8394	0.2412	0.8557	0.2196	0.77935	-0.0083
0.62	3.039	0.8765	0.0258	-0.0597	0.132	12.14	6	6.141	11.398	0.2095	0.8623	0.2211	0.90976	-0.0083
0.72	3.529	0.8765	0.0258	-0.0597	0.116	10.54	6	4.546	12.999	0.1857	0.8664	0.2235	1.0424	-0.0083
0.82	4.019	0.8765	0.0258	-0.0597	0.103	9.313	6	3.313	14.625	0.1673	0.8691	0.2264	1.17648	-0.0083
0.92	4.509	0.8765	0.0258	-0.0597	0.092	8.334	6	2.334	16.269	0.1525	0.8709	0.2297	1.31154	-0.0083
1.02	5	0.8765	0.0258	-0.0597	0.084	7.539	6	1.539	17.926	0.1405	0.8723	0.2332	1.4473	-0.0083

Table A2 Geometrical Properties of Blade Elements obtained from initial program for Tip speed ratio λ=6.

r	λ_r	C_L	C_D	Cm	c_e	φ_r (deg)	α (deg)	θ_T	V	C_y	C_z	dF_t	dF_d	dM
0.12	0.705	0.8765	0.0258	-0.0597	0.225	36.521	6	30.521	6.709	0.542	0.719	0.336	0.446	-0.0083
0.22	1.294	0.8765	0.0258	-0.0597	0.199	25.129	6	19.129	7.592	0.395	0.804	0.277	0.565	-0.0083
0.32	1.882	0.8765	0.0258	-0.0597	0.160	18.652	6	12.659	9.405	0.304	0.838	0.265	0.730	-0.0083
0.42	2.470	0.8765	0.0258	-0.0597	0.131	14.690	6	8.690	11.514	0.247	0.854	0.263	0.910	-0.0083
0.52	3.0588	0.8765	0.0258	-0.0597	0.109	12.06	6	6.069	13.754	0.208	0.862	0.265	1.098	-0.0083
0.62	3.647	0.8765	0.0258	-0.0597	0.094	10.22	6	4.222	16.064	0.180	0.867	0.269	1.289	-0.0083
0.72	4.235	0.8765	0.0258	-0.0597	0.082	8.856	6	2.856	18.416	0.160	0.870	0.273	1.482	-0.0083
0.82	4.823	0.8765	0.0258	-0.0597	0.072	7.808	6	1.808	20.794	0.144	0.871	0.278	1.678	-0.0083
0.92	5.411	0.8765	0.0258	-0.0597	0.065	6.979	6	0.979	23.190	0.132	0.873	0.283	1.874	-0.0083
1.02	6	0.8765	0.0258	-0.0597	0.059	6.308	6	0.308	25.599	0.121	0.874	0.288	2.070	-0.0083

Table A3 Geometrical Properties of Blade Elements obtained from initial program for Tip speed ratio λ=7.

r	λ_r	C_L	C_D	Cm	c_e	φ_r (deg)	α (deg)	θ_T	V	C_y	C_z	dF_t	dF_d	dM
0.12	0.8235	0.8765	0.0258	-0.0597	0.1925	33.685	6	27.685	7.8467	0.5075	0.7436	0.3686	0.5400	-0.0083
0.22	1.5098	0.8765	0.0258	-0.0597	0.1578	22.345	6	16.345	9.5701	0.3570	0.8204	0.3163	0.7267	-0.0083
0.32	2.1960	0.8765	0.0258	-0.0597	0.1232	16.321	6	10.321	12.259	0.2710	0.8484	0.3075	0.9626	-0.0083
0.42	2.8823	0.8765	0.0258	-0.0597	0.0990	12.755	6	6.7557	15.252	0.2186	0.8605	0.3087	1.2148	-0.0083
0.52	3.5686	0.8765	0.0258	-0.0597	0.0822	10.435	6	4.4359	18.379	0.1841	0.8666	0.3132	1.4743	-0.0083
0.62	4.2549	0.8765	0.0258	-0.0597	0.0700	8.8172	6	2.8172	21.577	0.1598	0.8700	0.3192	1.7376	-0.0083
0.72	4.9411	0.8765	0.0258	-0.0597	0.0608	7.6273	6	1.6273	24.817	0.1419	0.8721	0.3259	2.0033	-0.0083
0.82	5.6274	0.8765	0.0258	-0.0597	0.0538	6.7175	6	0.7175	28.084	0.1281	0.8735	0.3331	2.2705	-0.0083
0.92	6.3137	0.8765	0.0258	-0.0597	0.0481	6.0000	6	0.3512	31.36	0.1172	0.8743	0.3405	2.5387	-0.0083
1.02	7	0.8765	0.0258	-0.0597	0.0435	5.4200	6	0	34.666	0.1084	0.8750	0.3480	2.8075	-0.0083

Appendix III

Newmark Time Integration scheme

Time Integration schemes are methods to find the discrete time responses. Newmark method of time integration belongs to discrete time interval type where the discrete time responses are obtained by giving input of the Global Mass, Stiffness, Damping Matrices and Force vectors as inputs for solving the time domain response.

The Velocity is expressed as:

$$\{\dot{X}_{t+dt}\} = \{\dot{X}_t\} + [(1-\delta_n)\{\ddot{X}_t\} + \delta_n \{\ddot{X}_{t+dt}\}\Delta t] \quad \text{(A.8)}$$

The Displacement is expressed as:

$$\{X_{t+dt}\} = \{X_t\} + \{\dot{X}_t\}\Delta t + \left[\left(\frac{1}{2}-\alpha\right)\{\ddot{X}_t\} + \alpha\{\ddot{X}_{t+dt}\}\right] \quad \text{(A.9)}$$

The governing differential equations will be:

$$M_e \ddot{X}_{t+dt} + C_e \dot{X}_{t+dt} + K_e X_{t+dt} = F_{t+dt} \quad \text{(A.10)}$$

The procedure to develop the Velocity and Acceleration responses is as shown below:

Step 1:

The Mass$[M]_e$, Stiffness$[K]_e$ and Coupling matrices$[C]_e$ are taken.

Step 2:

The values of initial displacement $\{X_0\}$ and velocity $\{\dot{X}_0\}$ are given.

Step 3:

By choosing the values of *dt*, α and δ_n, the values of constants a_0 to a_7 are calculated as:

$$a_o = \frac{1}{\alpha(dt)^2},\ a_1 = \frac{\delta_n}{\alpha(dt)},\ a_2 = \frac{1}{\alpha(dt)},\ a_3 = \frac{1}{2\alpha} - 1,$$

$$a_4 = \frac{\delta_n}{\alpha} - 1,\ a_5 = \frac{dt}{2}\left(\frac{\delta_n}{\alpha} - 2\right) \text{ and } a_6 = dt(1-\delta_n)$$

Step 4:

Form the effective stiffness matrix and effective load matrix as:

$$[K_{eff}] = [K] + a_0[M] + a_1[C] \tag{A.11}$$

$$\{\bar{f}_{t+dt}\} = \{f_t\} + [M](a_0\{X_t\} + a_2\{\dot{X}_t\} + a_3\{\ddot{X}_t\} + [C](a_1\{X_t\} + a_4\{\dot{X}_t\} + a_5\{\ddot{X}_t\})$$

Step 5:

Solve $\{X_{t+dt}\} = [K_{eff}]^{-1}\{\bar{f}_{t+dt}\}$

Step 6:

The acceleration and velocities at time t+dt can be written as:

$$\{\ddot{X}_{t+dt}\} = a_0(\{X_{t+dt}\} - \{X_t\}) - a_2\{\dot{X}_t\} - a_3\{\ddot{X}_t\} \tag{A.12}$$

$$\{\dot{X}_{t+dt}\} = \{\dot{X}_t\} + a_6\{\ddot{X}_t\} + a_7\{\ddot{X}_{t+dt}\} \tag{A.13}$$

Appendix IV

MATLAB codes of the computations done to find out the Geometric Mass, Stiffness matrices and Global Force vector, are presented below. Then code for conducting Newmark Integration to get dynamic response spectrum is also explained below.

III.1 MATLAB Code to Compute Global Mass and Stiffness Matrices

```
%Function to compute global Mass and Stiffness Matrices
function[GMr,GKr]=Global_Mass_Stiffness215()
clc
clear all
%Initialize the parameters such as Length, Area, Young's Modulus, density
of each blade element,
A=[8.36529 42.39464 30.70165 20.19344 13.74556 9.815455 7.311195 5.63727
4.47042 3.627475]*1e-4;
E=6*1e9;den=1400;
L=[12 10 10 10 10 10 10 10 10 10]*1e-2;
Iz=[5.56868 738.1311 450.626805 203.71994 95.493375 48.53348 26.79224
16.04464 10.07106 6.61904]*1e-8;
Iy=[5.56868 196.0412 53.74758 13.28684 4.2068 1.94449 1.071425 0.45722
0.278195 0.18105]*1e-8;
Iyz=[0 339.0584 130.5248 38.01509 11.8492 5.248325 2.661715 0.519385
0.15931 0.017845]*1e-8;
G=2.5424*1e9;
J=[11.13736 66.25 53.38538 94.18572 72.81243 55.32523 41.51267 30.71831
22.44229 16.11037 11.59907 8.17581]*1e-8;
GK=zeros(66,66);Gks=zeros(66,66);GM=zeros(66,66);GMs=zeros(66,66);

a=zeros(length(A));b=zeros(12);c=zeros(12);d=zeros(12);e=zeros(12);f=zeros(
12);g=zeros(12);h=zeros(12);i1=zeros(12);j=zeros(12);


for i=1:length(A)

     a=(A(i)*E)/L(i);
     b=(12*E*Iz(i))/(L(i)^3);
     c=(6*E*Iz(i))/(L(i)^2);
     d=(12*E*Iy(i))/(L(i)^3);
     e=(6*E*Iy(i))/(L(i)^2);
     f=G*J(i)/L(i);
     g=4*E*Iy(i)/L(i);
     h=2*E*Iy(i)/L(i);
     i1=4*E*Iz(i)/L(i);
     j=2*E*Iz(i)/L(i);
     l=(12*E*Iyz(i))/(L(i)^3);
     m=(6*E*Iyz(i))/(L(i)^2);
     n=(4*E*Iyz(i))/L(i);
     o=(2*E*Iyz(i))/L(i);
```

```
    K=[a 0 0 0 0 0 -a 0 0 0 0 0; 0 b l 0 -m c 0 -b -l 0 -m c;0 l d 0 -e m 0
-l -d 0 -e m;0 0 0 f 0 0 0 0 0 -f 0 0;0 -m -e 0 g -n 0 m e 0 h -o;0 c m 0 -
n i1 0 -c -m 0 -o j;-a 0 0 0 0 0 a 0 0 0 0 0;0 -b -l 0 m -c 0 b l 0 m -c;0
-l -d 0 e -m 0 l d 0 e -m;0 0 0 -f 0 0 0 0 0 f 0 0;0 -m -e 0 h -o 0 m e 0 g
-n;0 c m 0 -o j 0 -c -m 0 -n i1];

    r=(i-1)*6+1;
    Gks(r:r+11,r:r+11)=K;
    GK=GK+Gks;
    Gks=zeros(66,66);
end

for i=1:length(A)

    a=1/3;
    b=13/35;
    c=(Iy(i)+Iz(i))/(3*A(i));
    d=L(i)^2/105;
    e=(11*L(i))/210;
    f=1/6;
    g=9/70;
    h=(13*L(i))/420;
    j=(Iy(i)+Iz(i))/(6*A(i));
    l=L(i)^2/140;
    area=A(i);leng=L(i);
    M=[a 0 0 0 0 0 f 0 0 0 0 0;0 b 0 0 0 e 0 g 0 0 0 -h;0 0 b 0 -e 0 0 0 g
0 h 0;0 0 0 c 0 0 0 0 0 j 0 0;0 0 -e 0 d 0 0 0 -h 0 -l 0;0 e 0 0 0 d 0 h 0
0 0 -l;f 0 0 0 0 0 a 0 0 0 0 0;0 g 0 0 0 h 0 b 0 0 0 -e;0 0 g 0 -h 0 0 0 b
0 e 0;0 0 0 j 0 0 0 0 0 c 0 0;0 0 h 0 -l 0 0 0 e 0 d 0;0 h 0 0 0 -l 0 -e 0
0 0 d]*(den*area*leng);
    r=(i-1)*6+1;
    GMs(r:r+11,r:r+11)=M;
    GM=GM+GMs;
    GMs=zeros(66,66);

end

GKr=zeros(61,61);GMr=zeros(61,61);

%Gkr and Gmr are the reduced matrices after giving initial boundary
%conditions


for i=6:66
    for j=6:66
        GKr(i-5,j-5)=GK(i,j);
        GMr(i-5,j-5)=GM(i,j);
    end
end
```

III.2 Function to Compute Globalized Force Vector

```
%Function to compute the global force vector
function[GFv]=global_force215()
clear all
clc
dt=0.001;T=1;
F=zeros(12,1);GFv=zeros(61,length(dt:dt:T));
```

```
count=1;
for t=dt:dt:T

   GFv(:,count)=force_gen215(t);
   count=count+1;
end
%function to generate generalized force vector for a particular time period
function[GFr]=force_gen215(t)
A=[8.36529 42.39464 30.70165 20.19344 13.74556 9.815455 7.311195 5.63727
4.47042 3.627475]*1e-4;
L=[12 10 10 10 10 10 10 10 10 10]*1e-2;
den_a=1.225;den=1400;
ome=50;
x=[0 0.12 0.22 0.32 0.42 0.52 0.62 0.72 0.82 0.92 1.02];
g=9.81;
Fks=zeros(66,1);GFv=zeros(66,1);
Cy=[0 0.468969449 0.350179036 0.276010116 0.227869405 0.194719307
0.170689529 0.152540617 0.138378381 0.127033037];
Cz=[0 0.762117034 0.821603907 0.846550333 0.858454545 0.864843104
0.868593723 0.870949967 0.872509192 0.873583902];
c=[1.631795 21.21254432 17.98410485 14.59462041 12.05483529 10.19619802
8.805764814 7.736053205 6.891462789 6.209478139]*1e-2;
Vr=[0 6.709276501 7.592497881 9.405770927 11.51439555 13.75465549
16.06476931 18.41629808 20.79435991 23.1904253 25.59925995];
Cm=[0 -0.0597 -0.0597 -0.0597 -0.0597 -0.0597 -0.0597 -0.0597 -0.0597 -
0.0597];
Iyz=[0 339.058415 130.524795 38.01509 11.8492 5.248325 2.661715 0.519385
0.15931 0.017845]*1e-8;

for i=1:length(A)

        if i==1
            F=zeros(12,1);
        else
           ti=ome*t*pi/180;
        a=(1/6)*den*L(i)*ome*ome*A(i)*(2*x(i)+x(i+1))-
      0.5*den*g*L(i)*A(i)*sin(ti);
        b=(1/4)*den_a*L(i)*Cy(i)*c(i)*Vr(i)*Vr(i)-
      0.5*den*g*L(i)*A(i)*cos(ti);
        d=(1/4)*den_a*L(i)*Cz(i)*c(i)*Vr(i)*Vr(i);
        e=(1/4)*den_a*L(i)*Cm(i)*c(i)*c(i)*Vr(i)*Vr(i)-
      0.5*den*L(i)*ome*ome*Iyz(i);
        f=0;
        h=0;
        j=(1/6)*den*L(i)*ome*ome*A(i)*(x(i)+2*x(i+1))-
      0.5*den*g*L(i)*A(i)*sin(ti);
        k=(1/4)*den_a*L(i)*Cy(i)*c(i)*Vr(i)*Vr(i)-
      0.5*den*g*L(i)*A(i)*cos(ti);
        l=(1/4)*den_a*L(i)*Cz(i)*c(i)*Vr(i)*Vr(i);
        m=(1/4)*den_a*L(i)*Cm(i)*c(i)*c(i)*Vr(i)*Vr(i)-
      0.5*den*L(i)*ome*ome*Iyz(i);
        n=0;
        o=0;

        F= [a;b;d;e;f;h;j;k;l;m;n;o];
        end

        rec=(i-1)*6+1;
        Fks(rec:rec+11,1)=F;
        GFv=GFv+Fks;
```

```
        Fks=zeros(66,1);
end

GFr=zeros(61,1);

for i=6:66
        GFr(i-5,1)=GFv(i,1);
end
```

III.3 Program of Implementing Newmark Method to conduct Dynamic Response Analysis

```
%Program to conduct Newmark Double Integration Analysis to find out
%Frequency Reponse of the Blade acted upon by various loads.
clc
clear all
dt=0.001;
T=1;
GF=zeros(61,length(dt:dt:T));
GM=zeros(61,61);
GK=zeros(61,61);F0=zeros(61,1);

[GM,GK]=Global_Mass_Stiffness215();
GF=global_force215();
F0=force_gen215(0);
X0=zeros(61,1);
X0d=zeros(61,1);
X0dd=inv(GM)*(F0-GK*X0);

delta=0.5;
alpha=0.25*(0.5+delta)^2;
c0=1/(alpha*dt*dt);
c1=delta/(alpha*dt);
c2=1/(alpha*dt);
c3=1/(2*alpha)-1;
c4=delta/alpha-1;
c5=(dt*(delta/alpha-2))/2;
c6=dt*(1-delta);
c7=delta*dt;

Keff=zeros(60,60);
Keff=GK+c0*GM;
Kinv=inv(Keff);

i=1;
X(:,1)=X0; Xd(:,1)=X0d; Xdd(:,1)=X0dd; t=0;

for t=dt:dt:T

        i=i+1;
        F=GF(:,i-1);
        Feff=F+GM*(c0*X(:,i-1)+c2*Xd(:,i-1)+c3*Xdd(:,i-1));

        X(:,i)=Kinv*Feff;
        Xdd(:,i)=c0*(X(:,i)-X(:,i-1))-c2*Xd(:,i-1)-c3*Xdd(:,i-1);
```

```
        Xd(:,i)=Xd(:,i-1)+c6*(Xdd(:,i-1))+c7*Xdd(:,i);

     F=zeros(61,1);Feff=zeros(61,1);
end


N=length(0:0.001:1);
fs=30;%62.5 samples per second
fnyquist=fs/2; %Nyquist frequency
X_mags=abs(fft(X(56,:)));
bin_vals=[0:N-1];
fax_Hz=bin_vals*fs/N;
N_2=ceil(N/2);

subplot(2,1,1)

plot(fax_Hz(1:N_2),X_mags(1:N_2))
xlabel('Frequency HZ')
ylabel('Magnitude')
title('Single sided maginitude spectrum');
axis tight

subplot(2,1,2)
plot(0:dt:T,X(58,:));
xlabel('time (in sec)')
ylabel('flexure angle response gamma')
title('Flapwise beating at the blade end')
axis tight
```